bioRxiv preprint doi: https://doi.org/10.64898/2026.02.12.705519; this version posted February 12, 2026. The copyright holder for this preprint (which was not certified by peer review) is the author/funder, who has granted bioRxiv a license to display the preprint in perpetuity. It is made available under aCC-BY 4.0 International license.

Complete definition of how mutations affect antibodies used to prevent RSV

Cassandra A.L. Simonich[1,2,3], Teagan E. McMahon[1], Lucas Kampman[1], Helen Y. Chu[4], Jesse D. Bloom[1,5*]

1. Basic Sciences and Computational Biology Divisions, Fred Hutchinson Cancer Center, Seattle, WA 98109, USA
2. Department of Pediatrics, University of Washington, Seattle, WA 98195, USA
3. Pediatric Infectious Diseases Division, Seattle Children's Hospital, Seattle, WA 98105, USA
4. Division of Allergy and Infectious Diseases, University of Washington School of Medicine, Seattle, WA 98195, USA
5. Howard Hughes Medical Institute, Seattle, WA 98109, USA

* correspondence to jbloom@fredhutch.org

Abstract

New antibodies targeting the F protein of respiratory syncytial virus (RSV) have substantially reduced infant hospitalizations. However, viral resistance is a concern: one antibody failed clinical trials due to emergence of a resistant strain, and sporadic resistance mutations to the most widely used antibody (nirsevimab) have been identified in breakthrough infections. Here we define how RSV F mutations affect antibody neutralization. We first provide a biophysical model of how the buffering effect of bivalent IgG binding combines with differences in monovalent Fab potency to explain why nirsevimab resistance mutations are more common in subtype B than subtype A RSV strains. We then perform pseudovirus deep mutational scanning to safely measure how nearly all mutations to F affect its cell entry function and neutralization by the IgG and Fab forms of nirsevimab, clesrovimab, and several other key antibodies. We use these measurements to enable real-time surveillance of RSV sequences for antibody resistance, and identify rare strains with sporadic resistance mutations. Overall, our work improves understanding of the mechanisms by which viral mutations impact antibody neutralization, enables monitoring for natural RSV strains resistant to antibodies of public-health importance, and can help guide development of future antibodies with resilience to viral escape.

bioRxiv preprint doi: https://doi.org/10.64898/2026.02.12.705519; this version posted February 12, 2026. The copyright holder for this preprint (which was not certified by peer review) is the author/funder, who has granted bioRxiv a license to display the preprint in perpetuity. It is made available under aCC-BY 4.0 International license.

Introduction

Respiratory syncytial virus (RSV) is the leading cause of infant hospitalization in the United States and second-leading cause of infant mortality globally[1–4]. Two highly potent, extended half-life monoclonal antibodies, nirsevimab and clesrovimab, are now licensed and recommended for the prevention of severe RSV disease in young infants[5–10]. Nirsevimab has demonstrated ~75-80% effectiveness against RSV-associated hospitalizations of infants[11–14] and (along with maternal vaccination) has appreciably reduced the number of infants hospitalized in countries where it is widely used[15]. Additional antibodies are under development including for low- and middle-income countries where RSV is a major cause of infant mortality[16–19].

Nirsevimab and clesrovimab target the prefusion conformation of the RSV fusion protein (F)[20–22]. While F is less variable than the surface proteins of influenza and SARS-CoV-2, it still evolves sufficiently fast to pose challenges for monoclonal antibodies[23–25]. Regeneron's anti-F antibody suptavumab failed a Phase 3 clinical trial because it was escaped by mutations in circulating RSV-B strains[26]. While nirsevimab has now been in use in the United States for two years and retained high effectiveness through the second season, sporadic strains with resistance mutations have been identified, particularly in breakthrough infections of individuals who had received the antibody[25,27–34]. It is unknown whether more resistant variants will emerge with broader use of monoclonal antibodies, which makes surveillance of RSV sequences for potential escape mutations an important public health priority[28,32,34–46]. However, surveillance is hindered by incomplete knowledge of how F mutations affect key antibodies, as prior studies have identified only a limited set of resistance mutations by passaging lab-adapted RSV in the presence of antibody[22,30,47] or looking for mutations in antibody binding footprints[28,30–32,34].

Here we provide a complete quantitative understanding of how RSV mutations affect antibodies by combining a biophysical model of bivalent IgG neutralization with deep mutational scanning measurements of how all possible amino-acid mutations affect F's cell entry function and neutralization by the IgG and Fab forms of key antibodies. Our work explains why nirsevimab resistance mutations are more common in one of the two RSV subtypes, defines the potential for escape from existing and candidate future clinical antibodies, and provides an experimentally-informed sequence surveillance platform to rapidly identify antibody-resistant natural RSV strains.

bioRxiv preprint doi: https://doi.org/10.64898/2026.02.12.705519; this version posted February 12, 2026. The copyright holder for this preprint (which was not certified by peer review) is the author/funder, who has granted bioRxiv a license to display the preprint in perpetuity. It is made available under aCC-BY 4.0 International license.

Results

Known nirsevimab resistance mutations differentially impact RSV subtypes A and B due to buffering by bivalent antibody binding

Clinical surveillance of individuals who received prophylaxis and experimental studies performed for resistance analysis for FDA licensure have found that viral mutations that escape nirsevimab are more common and impactful in subtype B than subtype A RSV strains[25,27–34]. This difference has been puzzling, since nirsevimab has a near-identical binding footprint on the F proteins of subtypes A and B[21], which have similar structures[20,48] and ~90% protein sequence identity[49].

We hypothesized that the greater prevalence and impact of escape mutations in RSV B is because nirsevimab binds with lower affinity to the F from subtype B versus subtype A[33,50]. IgG antibodies, which are produced by the human body and are also the form in which nirsevimab is administered, have two arms that can bind to the viral antigen, but antibodies can also be artificially produced in a Fab form with just one binding arm. We built a biophysical model of how mutations that reduce the monovalent Fab affinity of an antibody for a viral antigen impact neutralization by both Fab and bivalent IgG (Supplementary Appendix). The key insight of this model is that when an antibody's Fab affinity is sufficiently high, viral mutations that decrease Fab affinity do not measurably decrease IgG neutralization because bivalent binding keeps nearly all the IgG bound to even the mutant virus[51–53] (Figure 1A). We used the model to predict how the IgG and Fab forms of an antibody would neutralize a virus to which the Fab had high or moderate affinities, using parameter estimates that roughly reflect nirsevimab against RSV subtypes A and B (Figure 1B).

We then experimentally measured nirsevimab's neutralization of pseudovirus expressing RSV F from subtype A or B with two previously described nirsevimab escape mutations K68Q and (K/N)201S[28] (Figure 1C). The F-protein mutations reduced Fab neutralization of both subtypes A and B but only reduced IgG neutralization for subtype B, and the experimental data were consistent with the biophysical model (Figure 1B,C). These results suggest that nirsevimab escape mutations are more prevalent and impactful in subtype B than A because bivalent IgG binding buffers viral mutations in subtype A due to nirsevimab's higher affinity for that subtype[33,50]. A corollary, which we build on in this paper, is that it can be more generalizable across viral strains to measure how mutations affect Fab as well as IgG neutralization, since the buffering effect of bivalent binding manifests for IgG but not Fab.

bioRxiv preprint doi: https://doi.org/10.64898/2026.02.12.705519; this version posted February 12, 2026. The copyright holder for this preprint (which was not certified by peer review) is the author/funder, who has granted bioRxiv a license to display the preprint in perpetuity. It is made available under aCC-BY 4.0 International license.

Experimental measurements of functional constraint on all F mutations

To quantify the constraint on RSV F, we measured how nearly all amino-acid mutations to F's ectodomain affect its ability to mediate virion cell entry. To do this, we used pseudovirus deep mutational scanning[54] to quantify the ability of each mutant to enable F-pseudotyped lentiviral particles to infect 293T cells expressing the TIM1 attachment factor[55] (see Methods and Supplemental Figures 1 and 2). These pseudoviruses encode no viral proteins other than F and so can only undergo a single round of cell entry, making them a safe tool to study mutations to F without the use of actual pathogenic virus. We performed the deep mutational scanning using F from the lab-adapted subtype A strain of RSV termed "Long" after the name of the patient from whom it was isolated in the 1950s[56]. We created two independent F-expressing pseudovirus libraries, each of which contained nearly all possible amino-acid mutations to F's ectodomain (Supplemental Figure 1). Most F mutants contained just a single amino-acid mutation, although some contained no or multiple mutations (Supplemental Figure 1). We quantified the effects of mutations as the log2 cell entry of each mutant relative to the unmutated F, using global epistasis models[57,58] to jointly analyze the single and multi-mutant data. Negative values indicate a mutation impairs cell entry, while positive values indicate it improves cell entry.

Measurements of how all mutations affect F's cell entry function are shown in Figure 2A and the interactive plots at https://dms-vep.org/RSV_Long_F_DMS/cell_entry.html. As expected, variants with only synonymous mutations had wildtype-like cell entry scores of zero, variants with stop codon mutations had highly negative scores, and variants with amino-acid mutations had scores ranging from wildtype-like to highly negative (Supplemental Figure 2B). We performed three experimental replicates with each of the two independent libraries, and the measured cell entry effects were highly correlated across replicates and libraries (Supplemental Figure 2C-D); we report the average across all replicates for both libraries. We validated that the deep mutational scanning measurements were highly correlated with the infectious titer of pseudoviruses expressing individual F mutations spanning a range of effects (r = 0.92; Figure 2B).

Many regions of the F protein including the fusion peptide are highly constrained with most mutations deleterious for cell entry (Figure 2A). The p27 fragment is cleaved from the mature protein to yield the active form of F; the basic residues comprising the cleavage motifs at each end of p27 are intolerant to mutations whereas the cleaved p27 fragment itself is tolerant to mutations (Figure 2A). The epitope targeted by nirsevimab at the apex of the trimer is more mutationally tolerant than the epitope targeted by clesrovimab on the lateral face of the trimer (Figure 2C-D). Of the broadly defined antigenic regions[59,60], region 0 is the most mutationally tolerant whereas regions III and IV are more constrained (Figure 2E).

bioRxiv preprint doi: https://doi.org/10.64898/2026.02.12.705519; this version posted February 12, 2026. The copyright holder for this preprint (which was not certified by peer review) is the author/funder, who has granted bioRxiv a license to display the preprint in perpetuity. It is made available under aCC-BY 4.0 International license.

Most F mutations observed in natural RSV sequences relative to the lab-adapted parental strain used in our deep mutational scanning are measured to have minimal impact on cell entry (Supplemental Figure 3), as expected since there is strong natural selection for F to retain its cell entry function. The main exception is that cell entry is impaired by two mutations (S99N and T101P) that revert sites near an F proteolytic cleavage motif from their identities in the lab-adapted strain to amino acids commonly observed in natural sequences (Supplemental Figure 3). This exception highlights the fact that there can be discrepancies between how mutations affect pseudovirus entry in cell culture versus real-world viral fitness: presumably the N99 and P101 identities in natural sequences are better for authentic viral infection of human airway cells even if S99 and T101 give better pseudovirus entry into a cell line in the lab.

Measurement of how all F mutations affect nirsevimab neutralization

We next measured how all functionally tolerated F mutations affect neutralization by the antibody nirsevimab, which was the first antibody widely approved for RSV prophylaxis for infants[5,6,9,10]. We made these measurements by incubating the pseudovirus libraries with a range of antibody concentrations and quantifying the ability of each variant to infect cells at each antibody concentration, converting sequencing counts to fraction pseudovirus infectivity at each concentration using a spike-in standard (Supplemental Figure 4A)[54]. We measured the effects of mutations on neutralization by both IgG and Fab forms of nirsevimab, since the biophysical model described above suggests that Fab measurements are more generalizable across genetic backgrounds due to the absence of affinity-dependent buffering of bivalent IgG neutralization. We made two replicate measurements for each of the two independent pseudovirus libraries; throughout we report the average across replicates.

The mutations that affect neutralization by nirsevimab are at a subset of sites from 64 to 73 and 201 to 216 (Figure 3A-B and interactive plots at https://dms-vep.org/RSV_Long_F_DMS/nirsevimab_neutralization.html). These sites are all in or near the structurally determined nirsevimab binding site (Figure 3C). Some mutations at these sites (eg, 64T, 65E, 68Q/N/E, 201S/T, 203I, 208S/D/Y) have been previously shown to affect nirsevimab neutralization[25,27–31,33,47] or fusion inhibition (eg, 64M/65R, 64V/65E, 68I, 204S, 205S, 208I/K/Y)[32,34]. However, our deep mutational scanning identified numerous mutations that reduce neutralization that have not previously been reported in the literature, including mutations to additional amino-acid identities at sites 64, 65, 68, 201, 204, 205, 208 and 209 and mutations at sites not previously reported to affect nirsevimab neutralization, including 67, 73, 206-207, 210-211, and 215-216 (Figure 3B).

To validate the deep mutational scanning, we generated pseudoviruses carrying key mutations in F from the subtype A Long strain and measured their impact in neutralization assays with both nirsevimab IgG and Fab (Figure 3D). The effects of mutations on neutralization

bioRxiv preprint doi: https://doi.org/10.64898/2026.02.12.705519; this version posted February 12, 2026. The copyright holder for this preprint (which was not certified by peer review) is the author/funder, who has granted bioRxiv a license to display the preprint in perpetuity. It is made available under aCC-BY 4.0 International license.

IC50 were highly correlated with the deep mutational scanning (Figure 3E). Note that these assays validate the effect on nirsevimab neutralization of some of the resistance mutations newly identified by our deep mutational scanning (eg, 73N, 207E, 209D/Q, 210T, 211R, 215K).

To test if our deep mutational scanning of how mutations affect nirsevimab Fab neutralization of F from a subtype A strain could be extrapolated to a subtype B strain, we generated pseudoviruses carrying key mutations in the F of a subtype B strain (B1, a lab-adapted strain from the 1980s[61]). Most of the mutations that reduced Fab neutralization of the subtype A strain in the deep mutational scanning also reduced both Fab and IgG neutralization of the subtype B strain (Figure 3F and Supplemental Figure 4B-C). Consistent with the biophysical model in the first Results section, deep mutational scanning measurements of how subtype A mutations affect Fab neutralization correlate more strongly with both IgG and Fab neutralization of subtype B mutants than do deep mutational scanning measurements performed with IgG (Supplemental Figure 4C). The biophysical model also predicts that F mutations will cause a greater reduction in Fab than IgG neutralization for subtype A, but affect IgG and Fab neutralization similarly for subtype B since there is bivalent IgG buffering for the higher-affinity subtype A binding but not the lower-affinity subtype B binding; our measurements validate this prediction (Figure 3G). Note that S211R slightly increases subtype B neutralization despite decreasing subtype A neutralization for both Fab and IgG; for this mutation there must be additional background-specific differences between subtypes.

Our deep mutational scanning also identifies the F sequence differences responsible for the lower nirsevimab Fab potency to subtype B than subtype A. Most subtype A strains have N at site 67 and K at 209, while most subtype B strains have T at 67 and Q or R at 209. In the deep mutational scanning, N67T and K209Q reduce neutralization by nirsevimab Fab. We confirmed that mutating the subtype A F to the subtype B identities at these sites (N67T and K209Q) reduce neutralization by nirsevimab Fab, while the reverse mutations in subtype B (T67N and Q209K) increase neutralization (Supplemental Figure 4D). The effects of these swap mutations are much larger on Fab versus IgG neutralization, consistent with the biophysical model which posits that the nirsevimab affinity for F is sufficiently high that bivalent binding largely buffers mutation effects on IgG neutralization (Supplemental Figure 4D).

Measurement of how all F mutations affect clesrovimab neutralization

Clesrovimab, which targets a different region of F than nirsevimab, was recently approved as another option for RSV prevention for infants[5,7,9,10,62]. We measured the effects of F mutations on neutralization by clesrovimab IgG and Fab, performing two replicate deep mutational scanning experiments for each of the two independent pseudovirus libraries.

The mutations that most strongly affect clesrovimab neutralization occur at a subset of sites between 426-470 (Figure 4A-B). These sites are all within or near the structurally

bioRxiv preprint doi: https://doi.org/10.64898/2026.02.12.705519; this version posted February 12, 2026. The copyright holder for this preprint (which was not certified by peer review) is the author/funder, who has granted bioRxiv a license to display the preprint in perpetuity. It is made available under aCC-BY 4.0 International license.

determined clesrovimab binding site (Figure 4C and interactive plots at https://dms-vep.org/RSV_Long_F_DMS/clesrovimab_neutralization.html). Some mutations identified by our deep mutational scanning have been previously reported to affect clesrovimab neutralization (e.g., 443P, 445N, and 446E/R/W[22,62]). But we also identified a number of new mutations affecting clesrovimab, including additional mutations at sites 443, 445, and 446, as well as mutations at sites not previously associated with clesrovimab resistance, including 426, 429, 433, and 470 (Figure 4B).

To validate the deep mutational scanning, we generated pseudoviruses carrying key mutations in the context of F from both subtype A (Long strain) and subtype B (B1 strain) and measured their impact on neutralization by both clesrovimab IgG and Fab (Figure 4D-E). The effects of mutations on neutralization IC50 were highly correlated with the deep mutational scanning for both subtypes (Figure 4E).

Mutations that moderately reduce clesrovimab neutralization had a greater impact on Fab than IgG neutralization for both subtypes (Figure 4A,B,D; for example, R429M/S). This tendency for moderate-effect mutations to reduce Fab neutralization more than IgG neutralization is also observed for nirsevimab against subtype A but not subtype B (Figure 3G). These observations are consistent with the biophysical model of how bivalent IgG buffering reduces the impact of mutations on IgG neutralization when the Fab affinity is sufficiently high (which is true for clesrovimab against both subtypes A and B, but for nirsevimab only against subtype A). Indeed, unlike for nirsevimab, clesrovimab Fab has similarly high neutralization potencies against both subtypes (Supplemental Figure 5A), and the effects of mutations on clesrovimab neutralization are well correlated across subtypes (Supplemental Figure 5B).

Our deep mutational scanning found fewer sites where mutations strongly reduced clesrovimab neutralization compared to nirsevimab. Part of the reason may be differences in functional constraint: it is only possible to measure the impact on neutralization of F mutations that retain at least some cell entry function, and our deep mutational scanning shows that mutations in the clesrovimab epitope tend to be more deleterious to cell entry than mutations in the nirsevimab epitope (Figure 2C-D). Indeed, even among mutations that retain sufficient cell entry to measure their impact on neutralization, the ones that reduce clesrovimab neutralization tend to impair cell entry more than the ones that reduce nirsevimab neutralization (Supplemental Figure 5C). However, it should be noted that there are still some mutations that reduce clesrovimab neutralization without impairing cell entry.

Phenotypically-informed surveillance of natural RSV sequences for antibody resistance

Now that nirsevimab and clesrovimab are in widespread use, surveillance for natural RSV strains with resistance to these antibodies is a public-health priority[29,32,34]. However, although large numbers of human RSV infections are regularly being sequenced[28–30,32,34,37–39,45,46,63–66],

bioRxiv preprint doi: https://doi.org/10.64898/2026.02.12.705519; this version posted February 12, 2026. The copyright holder for this preprint (which was not certified by peer review) is the author/funder, who has granted bioRxiv a license to display the preprint in perpetuity. It is made available under aCC-BY 4.0 International license.

interpretation of these sequences has been limited by incomplete knowledge of which mutations affect antibody resistance. Our deep mutational scanning can help solve this problem by enabling immediate assessment of all RSV sequences for potential antibody resistance. Specifically, we calculated two escape scores for each RSV sequence: the summed effect on neutralization of all its F mutations relative to the subtype A Long strain used in the deep mutational scanning, and the effect of the single mutation that caused the greatest reduction in neutralization. We integrated these scores into Nextstrain[67] phylogenetic trees of RSV showing the latest sequence data from Pathoplexus[68]. Since Nextstrain subsamples the many available F sequences for effective visualization, we also created new builds that ensure that the subsampling includes sequences with high escape scores. Interactive phylogenetic trees that can be colored by the escape scores and are updated to include the latest available sequences are at https://nextstrain.org/rsv/b/F-antibody-escape/6y?c=Nirsevimab-Fab_total_escape. Static images based on further subsampled versions of these trees are shown in Figure 5A-B and Supplemental Figure 6A-B.

Sequences with high nirsevimab or clesrovimab escape scores were rare (<1% of all sequences) and distributed across the phylogenetic trees, suggesting resistance mutations have arisen sporadically and not undergone sustained spread (Figure 5A-B, Supplemental Figure 6A-B, and https://nextstrain.org/rsv/b/F-antibody-escape/6y?c=Nirsevimab-Fab_total_escape). However, the fact that strains with resistance to nirsevimab or clesrovimab have emerged and transmitted in humans to a limited extent underscores the importance of continued surveillance.

To validate that natural sequences with high escape scores had reduced neutralization, we generated RSV pseudoviruses expressing the F proteins from strains with high escape scores for either nirsevimab or clesrovimab. Nearly all strains with high escape scores had reduced neutralization by nirsevimab or clesrovimab relative to control recent subtype A or B strains with low escape scores (Figure 5C-D and Supplemental Figure 6C-D). The natural strains with reduced neutralization include ones with resistance mutations newly identified by our deep mutational scanning (eg K68E, K201I and K201E for nirsevimab, and R429S for clesrovimab). An important caveat is that the escape scores assume resistance can be predicted from the additive effects of a strain's mutations; our validation assays show that assumption usually holds, but we did identify one subtype A strain with a high nirsevimab escape score that did not have reduced neutralization, possibly due to an epistatic interaction of its S211R resistance mutation with a nearby R213S mutation (Supplemental Figure 6C).

Effect of mutations on neutralization by historical and candidate clinical antibodies

We next used deep mutational scanning to characterize mutations that affect neutralization by three additional antibodies of historical or potential future clinical relevance. Suptavumab failed a Phase 3 trial run from 2015 to 2017 due to a lack of efficacy against subtype B infections[26]. Our

bioRxiv preprint doi: https://doi.org/10.64898/2026.02.12.705519; this version posted February 12, 2026. The copyright holder for this preprint (which was not certified by peer review) is the author/funder, who has granted bioRxiv a license to display the preprint in perpetuity. It is made available under aCC-BY 4.0 International license.

deep mutational scanning shows that the mutations that cause the greatest reduction in suptavumab neutralization are at sites 173 and 174 (Figure 6A-B). Starting in 2015, the L172Q and S173L mutations became prevalent in subtype B sequences (Figure 6C), and the reduced ability of suptavumab to neutralize strains with these two mutations was ultimately found to have led to the failed clinical trial[26]. Our deep mutational scanning shows that S173L reduces suptavumab neutralization (Figure 6B) while having minimal adverse impact on F's cell entry function (Supplemental Figure 7A). Notably, S173L had already spread to roughly half of subtype B RSV sequences by the time the suptavumab Phase 3 clinical trial began in November of 2015[26], so its failure could have been anticipated if our deep mutational scanning had been available in advance.

We next profiled palivizumab, an older monoclonal antibody previously recommended only for high-risk (eg, pre-term) infants[69] that has now largely been replaced by nirsevimab and clesrovimab since they have a longer half life and are more potent. Our deep mutational scanning showed palivizumab neutralization is strongly reduced by mutations at a subset of sites from 255 to 277 (Supplemental Figure 7A-D), consistent with prior work showing mutations at some of these sites cause palivizumab resistance[24,70–74].

Finally, we applied deep mutational scanning to RSM01[16,47], a new highly potent antibody being developed for potential use in low and middle income countries where RSV is a leading cause of infant mortality. Mutations that reduce RSM01 neutralization occur at a subset of sites from 68-80 and 202-216 (Figure 6D-E). RSM01 targets a similar region of the RSV F trimer as nirsevimab[16,47], but there is only partial overlap of their resistance mutations: for instance, mutations at sites 201, 204 and 208 cause a greater reduction in nirsevimab than RSM01 neutralization (Figure 6E-F, Figure 3A-B and Supplemental Figure 7A). A recent study that serially passaged replicative RSV in the presence of RSM01 selected an I206T/N262Y double mutant with partial antibody resistance[47]; our deep mutational scanning finds that I206T reduces RSM01 neutralization.

Discussion

We have used pseudovirus deep mutational scanning to measure how nearly all mutations to RSV F affect neutralization by clinically relevant antibodies. Prior work to identify resistance mutations, including for FDA-required resistance analyses[33,62,75], has serially passaged authentic RSV in the presence of antibody[22,30,47]. Our strategy has two advantages over this classical approach: it characterizes all mutations rather than just identifying whichever ones stochastically arise during viral passage, and it does not generate mutants of actual replicative virus (pseudoviruses can only undergo a single round of cell entry). On the other hand, serial passaging can uncover resistance mediated by combinations of mutations, whereas deep

bioRxiv preprint doi: https://doi.org/10.64898/2026.02.12.705519; this version posted February 12, 2026. The copyright holder for this preprint (which was not certified by peer review) is the author/funder, who has granted bioRxiv a license to display the preprint in perpetuity. It is made available under aCC-BY 4.0 International license.

mutational scanning only measures the effects of single mutations. However, in practice our deep mutational scanning identified all resistance mutations previously reported by serial-passage studies as well as a number of new mutations, some of which have already been observed in natural RSV sequences.

At first blush, the fact that we measured effects of mutations to F from only a single subtype A strain might seem a major limitation, especially given the perplexing prior observation that nirsevimab resistance is more prevalent in subtype B[25,27–34]. But a key insight of our work is that subtype-dependent effects of mutations on nirsevimab neutralization are largely explained by biophysically modeling how bivalent IgG binding buffers mutations when Fab potency is sufficiently high. Because nirsevimab Fab has higher affinity for subtype A than subtype B RSV F[33,50], mutations that moderately reduce Fab neutralization of both subtypes only reduce IgG neutralization of subtype B. Therefore, we measured how F mutations affected both IgG and Fab neutralization, and showed that the Fab measurements identified mutations that reduced IgG neutralization of subtype B despite having minimal impact on IgG neutralization of subtype A. This general biophysical principle extends beyond RSV and nirsevimab, and implies that mutations that modulate Fab potency without affecting IgG neutralization can nonetheless alter the impact of subsequent mutations on IgG neutralization. However, although bivalent IgG buffering explains much of the subtype-dependent effects of F mutations on nirsevimab neutralization, other more specific mechanisms can also shape how a mutation impacts different strains, and so the fact that our measurements were performed in a single genetic background remains a caveat.

An immediate benefit of our work is enabling real-time assessment of natural RSV sequences for antibody resistance. Because anti-RSV antibodies are of such public-health importance, genomic surveillance of RSV has become a major priority[28,32,34–43]: there are now >60,000 sequences in public databases[68] and the number is rapidly growing. However, interpretation of these sequences has been limited by the fact that prior experimental work only characterized how a small fraction of all F mutations affect antibody neutralization[25,27–34,47,62]. We used our deep mutational scanning data to score all available sequences and identify sporadic nirsevimab or clesrovimab resistance, in some cases mediated by mutations not previously reported to impact those antibodies. We also implemented this resistance-scoring system into real-time Nextstrain phylogenetic trees (https://nextstrain.org/rsv/b/F-antibody-escape/6y?c=Nirsevimab-Fab_total_escape) and created a web interface with our experimental data (https://dms-vep.org/RSV_Long_F_DMS). These resources will enable continued assessment for resistance to current clinical antibodies as well as new ones under development like RSM01[16,47]. The tools developed here also can be applied to additional new candidate clinical antibodies[76] or antibody cocktails[77].

Fortunately, resistance to nirsevimab and clesrovimab is currently rare. Resistance could remain rare, or could eventually spread as happened with suptavumab resistance in RSV

bioRxiv preprint doi: https://doi.org/10.64898/2026.02.12.705519; this version posted February 12, 2026. The copyright holder for this preprint (which was not certified by peer review) is the author/funder, who has granted bioRxiv a license to display the preprint in perpetuity. It is made available under aCC-BY 4.0 International license.

subtype B in 2015-2016[26] or oseltamivir (Tamiflu) resistance in H1N1 influenza in 2008[78]. Resistance can spread incidentally if resistance mutations also enhance viral fitness by an unrelated mechanism like increasing transmissibility or reducing recognition by population immunity[79,80]; such incidental spread likely explains why suptavumub resistance emerged prior to Phase 3 clinical trials of that antibody. We have previously shown that some nirsevimab resistance mutations mildly reduce neutralization of RSV by polyclonal human sera[55], raising the possibility that they could confer a small incidental benefit to the virus. Now that nirsevimab and clesrovimab are in clinical use, there is also direct evolutionary pressure for viral resistance that enables infection of treated individuals. However the infants receiving these antibodies are just a small fraction (<1%) of all people[13,81]. Resistance would therefore confer a real but small advantage, and so such a strain would spread only if the resistance mutations do not impair other aspects of transmissibility by even a small amount[80]. It is impossible to experimentally measure RSV transmissibility with such precision; although our deep mutational scanning measured how mutations affect F's cell entry function, these experiments have a precision far worse than 1% and cell entry is only one of several F properties that contribute to transmissibility. Therefore, the best that can currently be done is to monitor for the real-world spread of resistance while continuing to develop new antibodies with distinct resistance profiles—both goals that our study helps advance.

Acknowledgements

We thank Richard Neher and James Hadfield for assistance with the Nextstrain visualizations. This work was supported by the NIAID/NIH (R01AI141707 to JDB, U19AI181767 subcontract to JDB) and the Gates Foundation (INV-072143). CALS is a fellow in the Pediatric Scientist Development Program and was supported in part by K12-HD000850 from the NICHD/NIH and Eunice Kennedy Shriver NICHD/NIH T32HD007233. JDB is an Investigator of the Howard Hughes Medical Institute. We gratefully acknowledge the authors, and the originating and submitting laboratories, for generating and sharing viral genome sequences and associated metadata via Pathoplexus at https://doi.org/10.62599/PP_SS_628.1, https://doi.org/10.62599/PP_SS_661.1, and https://doi.org/10.62599/PP_SS_662.1.

Competing Interests

JDB consults for Apriori Bio, Invivyd, the Vaccine Company, GSK, and Pfizer. JDB is an inventor on Fred Hutch licensed patents related to deep mutational scanning of viral proteins. HYC has served on advisory boards for Vir and Roche. The Bloom lab receives funding from Third Rock Ventures NewCo under a sponsored research agreement related to antibodies distinct from the ones analyzed in the current study.

bioRxiv preprint doi: https://doi.org/10.64898/2026.02.12.705519; this version posted February 12, 2026. The copyright holder for this preprint (which was not certified by peer review) is the author/funder, who has granted bioRxiv a license to display the preprint in perpetuity. It is made available under aCC-BY 4.0 International license.

Author Contributions

Conceptualization: CALS, TEM, HYC, JDB; Methodology: CALS, TEM, LK, JDB; Investigation: CALS, TEM; Data curation: CALS, TEM, JDB; Visualization: CALS, TEM, JDB; Writing-Original Draft: CALS, TEM, JDB; Writing-Review & Editing: all authors; Supervision: JDB; Funding Acquisition: CALS, JDB.

bioRxiv preprint doi: https://doi.org/10.64898/2026.02.12.705519; this version posted February 12, 2026. The copyright holder for this preprint (which was not certified by peer review) is the author/funder, who has granted bioRxiv a license to display the preprint in perpetuity. It is made available under aCC-BY 4.0 International license.

Main Figures

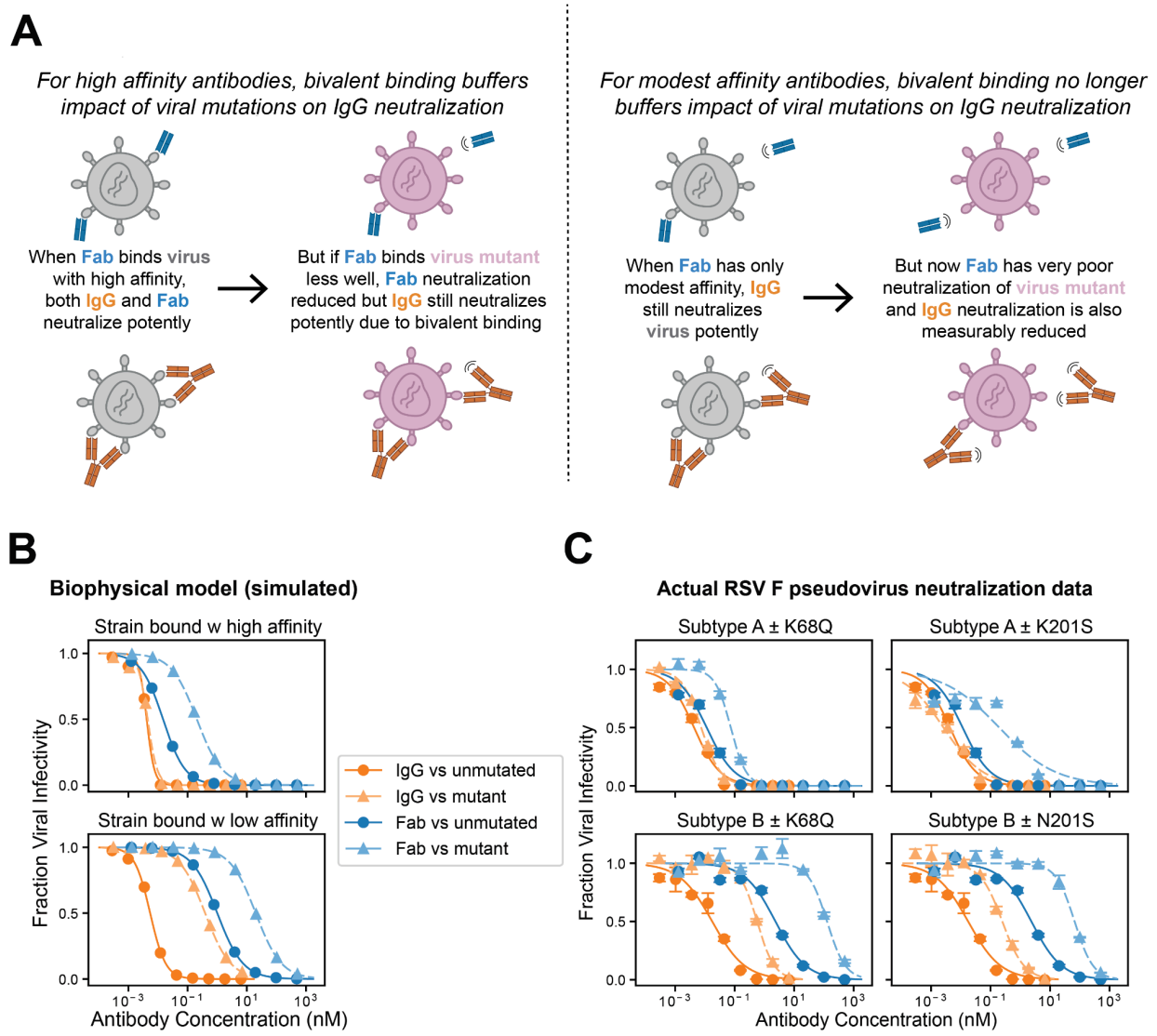

Figure 1. RSV F mutations cause more nirsevimab escape in subtype B versus subtype A because the ability of bivalent IgG binding to buffer mutations depends on Fab affinity.

(A) Bivalent IgG binding buffers the effects of mutations that reduce monovalent Fab affinity when the Fab has sufficiently high affinity for the viral antigen, but how this buffering vanishes if the Fab affinity is more modest. **(B)** Predictions of a quantitative biophysical model (see Supplementary Appendix) of how a viral mutation that reduces Fab affinity affects both IgG and Fab neutralization of a viral strain to which the Fab has high or low affinity. When the Fab has high affinity, mutations that reduce affinity do not appreciably reduce IgG neutralization.

bioRxiv preprint doi: https://doi.org/10.64898/2026.02.12.705519; this version posted February 12, 2026. The copyright holder for this preprint (which was not certified by peer review) is the author/funder, who has granted bioRxiv a license to display the preprint in perpetuity. It is made available under aCC-BY 4.0 International license.

(C) Experimental data showing how two known RSV subtype B nirsevimab escape mutations, K68Q and (K/N)201S, affect neutralization by nirsevimab IgG and Fab of pseudoviruses expressing RSV F from subtype A (Long strain) or subtype B (B1 strain). Nirsevimab has a higher affinity for subtype A than subtype B[33,50]. Consistent with the biophysical model, the mutations reduce Fab neutralization for both subtypes, but only reduce IgG neutralization for subtype B. Points represent the mean and standard error of replicate measurements.

bioRxiv preprint doi: https://doi.org/10.64898/2026.02.12.705519; this version posted February 12, 2026. The copyright holder for this preprint (which was not certified by peer review) is the author/funder, who has granted bioRxiv a license to display the preprint in perpetuity. It is made available under aCC-BY 4.0 International license.

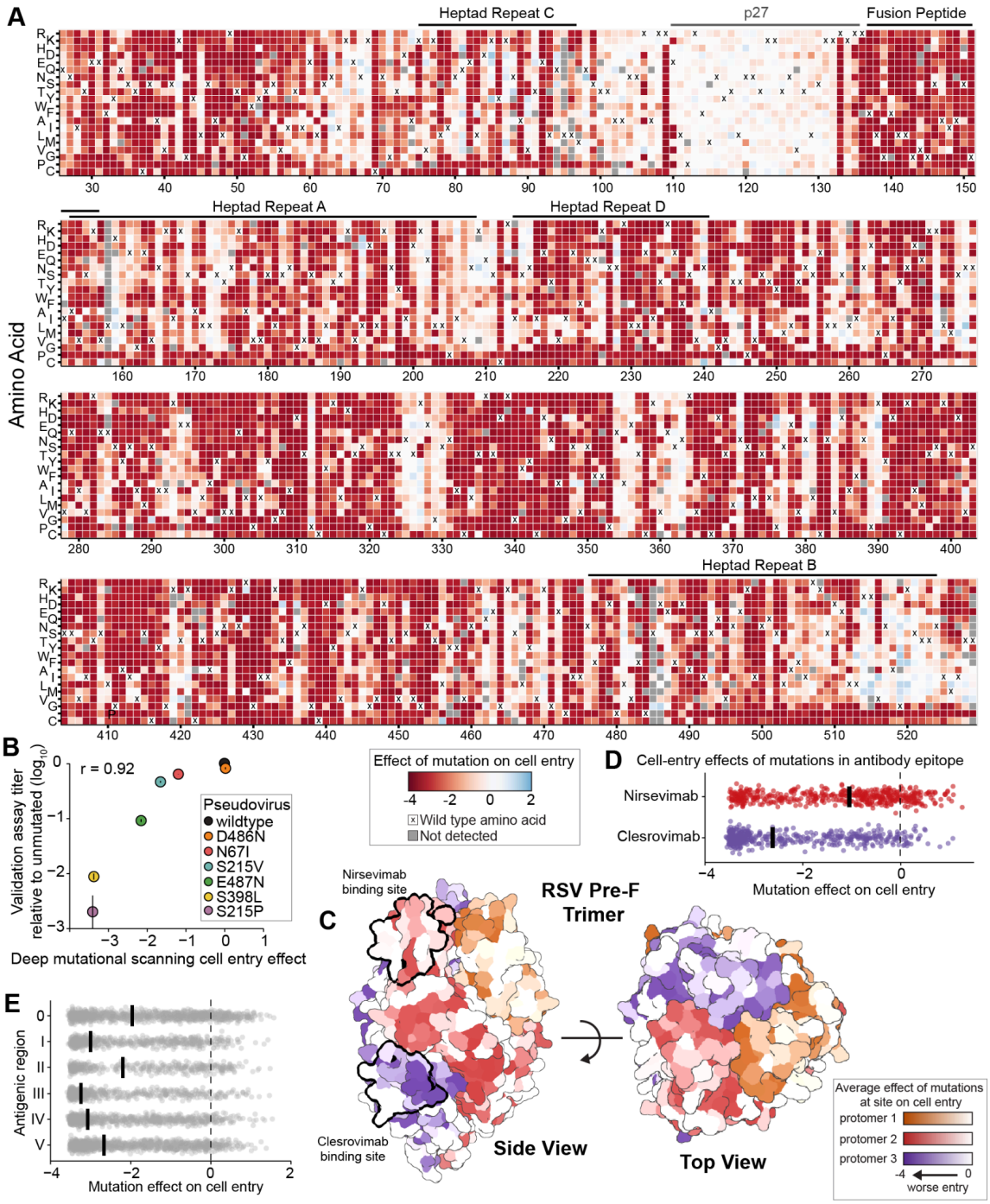

Figure 2. Effects of mutations to RSV F on its cell entry function

(A) Effects of single amino acid mutations on pseudovirus entry in 293T-TIM1 cells as measured by deep mutational scanning. Each box represents the effect of a specific mutation, with colors

bioRxiv preprint doi: https://doi.org/10.64898/2026.02.12.705519; this version posted February 12, 2026. The copyright holder for this preprint (which was not certified by peer review) is the author/funder, who has granted bioRxiv a license to display the preprint in perpetuity. It is made available under aCC-BY 4.0 International license.

indicating decreased (red), unchanged (white), or slightly increased (blue) cell entry relative to the unmutated F. Mutations not reliably measured in our experiments are indicated by gray boxes, and the wildtype amino acid in the parental subtype A Long strain at each site is indicated with an 'x'. See https://dms-vep.org/RSV_Long_F_DMS/cell_entry.html for an interactive version of this heatmap. **(B)** Correlation between mutation effects on cell entry measured by deep mutational scanning and pseudovirus titer in a validation assay using F single-mutant pseudoviruses. Each point represents the mean of two replicate measurements. **(C)** Average effect of mutations at each site mapped onto the prefusion F trimer structure (PDB 5UDC[21]), viewed from the top and side. Each protomer is colored with a separate color with darker shading indicating more deleterious effects on cell entry. The nirsevimab and clesrovimab binding footprints are outlined on one monomer of the trimer. **(D)** Distribution of mutation effects on cell entry at sites that comprise the epitopes of nirsevimab and clesrovimab (defined as residues that bury ≥5 Å^2 of surface area upon Fab binding). Each point represents the effect of an individual mutation (negative values indicate worse cell entry), and the thick black lines indicate the median. **(E)** Distribution of mutation effects on cell entry for mutations at sites that comprise broadly defined antigenic regions[59].

bioRxiv preprint doi: https://doi.org/10.64898/2026.02.12.705519; this version posted February 12, 2026. The copyright holder for this preprint (which was not certified by peer review) is the author/funder, who has granted bioRxiv a license to display the preprint in perpetuity. It is made available under aCC-BY 4.0 International license.

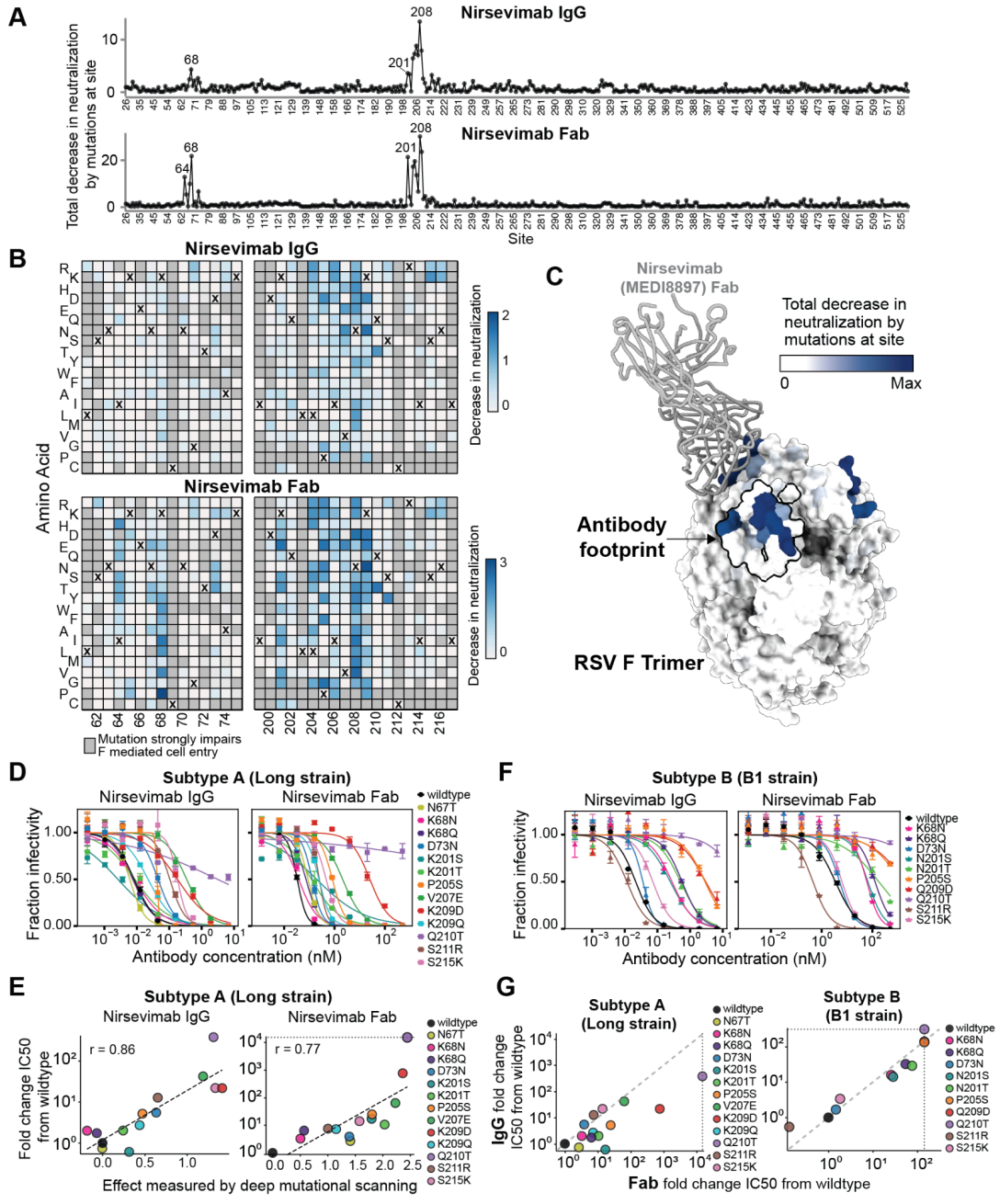

Figure 3. Effects of mutations to RSV F on neutralization by nirsevimab IgG and Fab

(A) Total decrease in neutralization from all mutations at each site for nirsevimab IgG or Fab as measured by deep mutational scanning. See

bioRxiv preprint doi: https://doi.org/10.64898/2026.02.12.705519; this version posted February 12, 2026. The copyright holder for this preprint (which was not certified by peer review) is the author/funder, who has granted bioRxiv a license to display the preprint in perpetuity. It is made available under aCC-BY 4.0 International license.

https://dms-vep.org/RSV_Long_F_DMS/nirsevimab_neutralization.html for interactive plots that show the effects of all mutations. **(B)** Heatmaps showing effects on neutralization of mutations within the epitope of nirsevimab. Each box represents the effect of a single mutation, with positive values indicating decreased neutralization. Dark gray indicates mutations that are too deleterious for cell entry to measure their effect on neutralization. The wildtype amino acid in the subtype A Long strain used for the deep mutational scanning at each site is indicated with an 'x'. **(C)** Pre-fusion RSV F trimer (PDB 5UDC[21]) in complex with nirsevimab Fab (gray cartoon) colored by the total effect of mutations at each site on neutralization by nirsevimab Fab. **(D)** Neutralization curves for nirsevimab IgG or Fab versus pseudovirus expressing the indicated mutants of the subtype A Long strain F. Curves for K68Q and K201T are duplicated from Figure 1. **(E)** Correlation of mutation effects on neutralization by nirsevimab in the neutralization assays versus deep mutational scanning for IgG or Fab for mutants of the subtype A Long strain F. Black dashed line shows the correlation line. Horizontal dashed line indicates limit of detection. **(F)** Neutralization curves for nirsevimab IgG or Fab versus pseudovirus expressing the indicated mutants of F from the subtype B strain B1. Curves for K68Q and N201T are duplicated from Figure 1. **(G)** Comparison of fold change in IC50 between nirsevimab IgG and Fab for mutations in subtype A background (Long strain) and subtype B background (B1 strain). Dashed gray lines show 1:1. Horizontal and vertical dashed lines indicate the limit of detection.

bioRxiv preprint doi: https://doi.org/10.64898/2026.02.12.705519; this version posted February 12, 2026. The copyright holder for this preprint (which was not certified by peer review) is the author/funder, who has granted bioRxiv a license to display the preprint in perpetuity. It is made available under aCC-BY 4.0 International license.

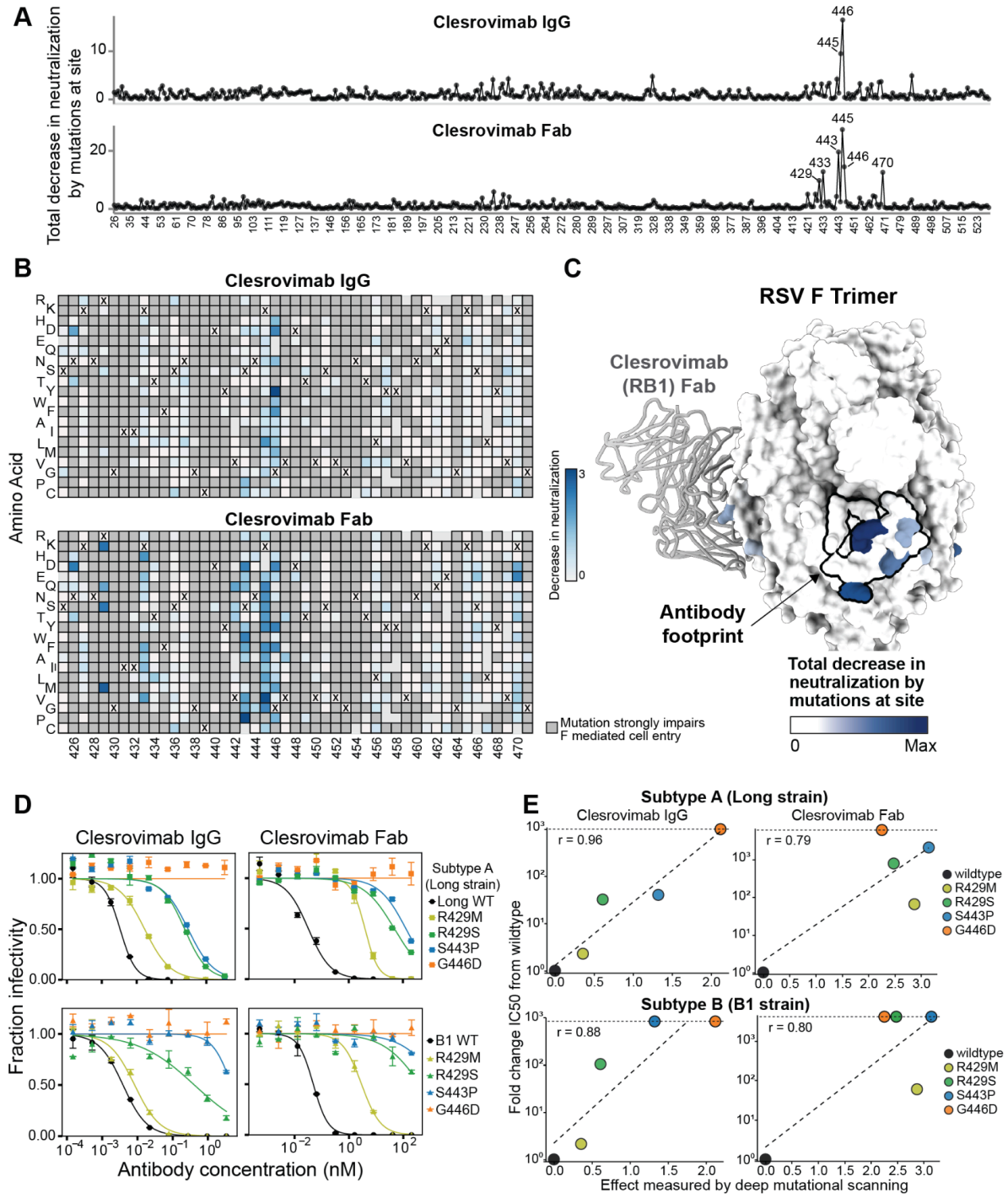

Figure 4. Effects of mutations to RSV F on neutralization by clesrovimab IgG and Fab

(A) Total decrease in neutralization from all mutations at each site for clesrovimab IgG or Fab as measured by deep mutational scanning. See

bioRxiv preprint doi: https://doi.org/10.64898/2026.02.12.705519; this version posted February 12, 2026. The copyright holder for this preprint (which was not certified by peer review) is the author/funder, who has granted bioRxiv a license to display the preprint in perpetuity. It is made available under aCC-BY 4.0 International license.

https://dms-vep.org/RSV_Long_F_DMS/clesrovimab_neutralization.html for interactive plots that show the effects of all mutations. **(B)** Heatmaps showing effects on neutralization of mutations within the epitope of clesrovimab. Each box represents the effect of a single mutation, with positive values indicating decreased neutralization. Dark gray indicates mutations that are too deleterious for cell entry to measure their effect on neutralization. Light gray shading indicates mutations that were not measured. The wildtype amino acid in the subtype A Long strain used for the deep mutational scanning at each site is indicated with an 'x'. **(C)** Pre-fusion RSV F trimer (PDB 6OUS[22]) in complex with clesrovimab Fab (gray cartoon) colored by the total effect of mutations at each site on neutralization by clesrovimab Fab. **(D)** Neutralization curves for clesrovimab IgG and Fab of pseudovirus expressing F with point mutations in subtype A (Long) or subtype B (B1) background. Individual mutations were selected to span a range of effects on neutralization. **(E)** Correlation of mutation effects on neutralization by clesrovimab IgG and Fab between deep mutational scanning and traditional pseudovirus neutralization assays with the indicated F mutants in subtype A (Long strain) or subtype B (B1 strain). Horizontal and vertical lines indicate limits of detection.

bioRxiv preprint doi: https://doi.org/10.64898/2026.02.12.705519; this version posted February 12, 2026. The copyright holder for this preprint (which was not certified by peer review) is the author/funder, who has granted bioRxiv a license to display the preprint in perpetuity. It is made available under aCC-BY 4.0 International license.

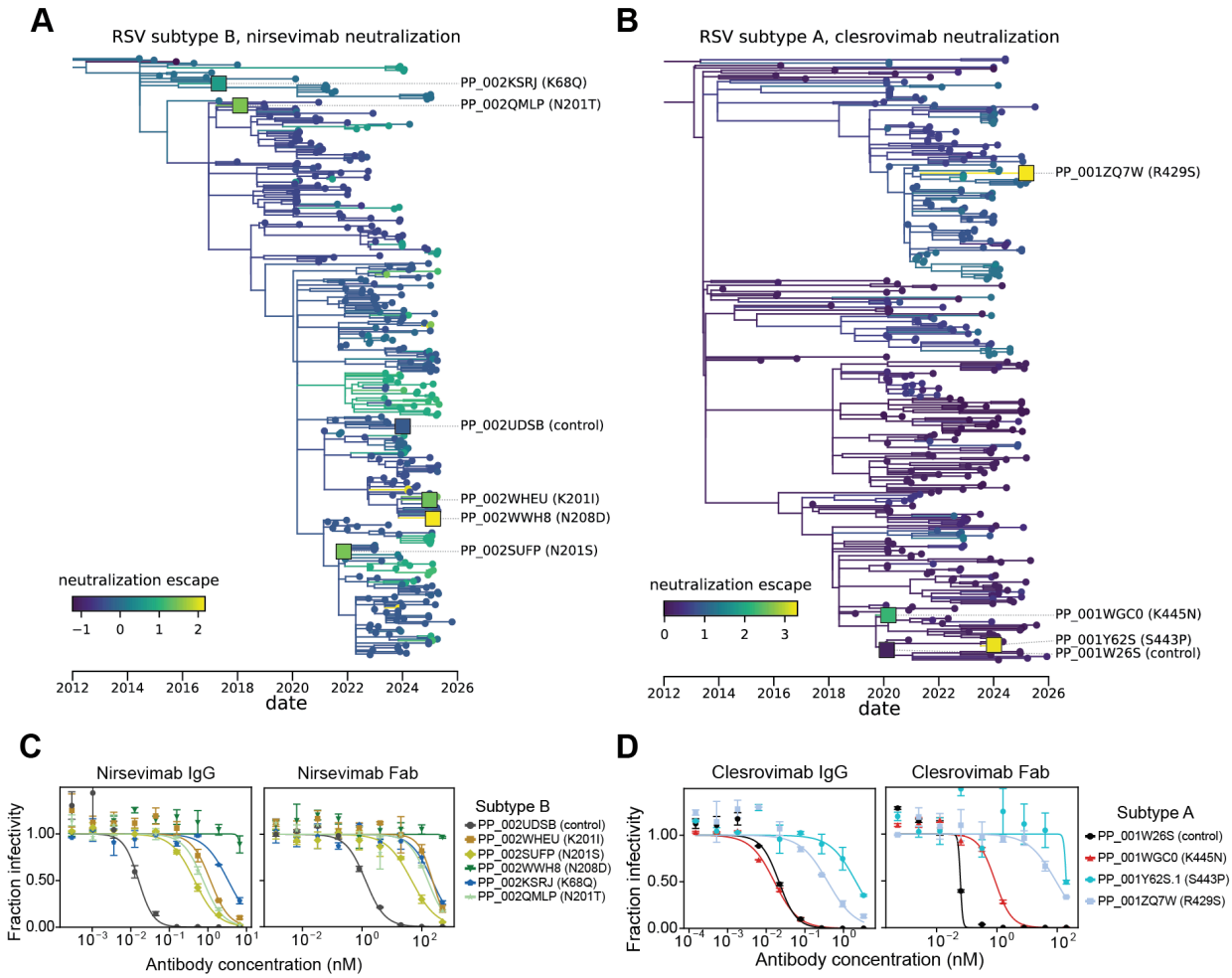

Figure 5. Sporadic natural RSV strains have reduced neutralization by nirsevimab or clesrovimab

(A) Phylogenetic trees of subtype B RSV F sequences colored by nirsevimab escape scores computed as the summed effects of all mutations as measured by the deep mutational scanning. Strains chosen for validation of nirsevimab neutralization are indicated by boxes and labeled with the Pathoplexus identifier and top resistance mutation. See https://nextstrain.org/rsv/b/F-antibody-escape/6y?c=Nirsevimab-Fab_total_escape for interactive Nextstrain trees that show more sequences and are updated in real time. **(B)** Tree of subtype A RSV F sequences colored by clesrovimab escape scores. **(C)** Neutralization curves showing nirsevimab IgG or Fab neutralization of pseudoviruses expressing F from the subtype B strains

bioRxiv preprint doi: https://doi.org/10.64898/2026.02.12.705519; this version posted February 12, 2026. The copyright holder for this preprint (which was not certified by peer review) is the author/funder, who has granted bioRxiv a license to display the preprint in perpetuity. It is made available under aCC-BY 4.0 International license.

labeled on the tree. The strains with high escape scores all have reduced neutralization relative to a control strain with a low escape score[55]. **(D)** Neutralization curves showing clesrovimab IgG or Fab neutralization of pseudoviruses expressing F from the subtype A strains labeled on the tree. Strains with high escape scores all have reduced neutralization relative to a control strain, except a strain (PP_001WGC0) with only a moderate escape score that shows reduced Fab not but not IgG. See Supplemental Figure 6 for trees and validating neutralization assays for subtype A strains with nirsevimab resistance and subtype B strains with clesrovimab resistance.

bioRxiv preprint doi: https://doi.org/10.64898/2026.02.12.705519; this version posted February 12, 2026. The copyright holder for this preprint (which was not certified by peer review) is the author/funder, who has granted bioRxiv a license to display the preprint in perpetuity. It is made available under aCC-BY 4.0 International license.

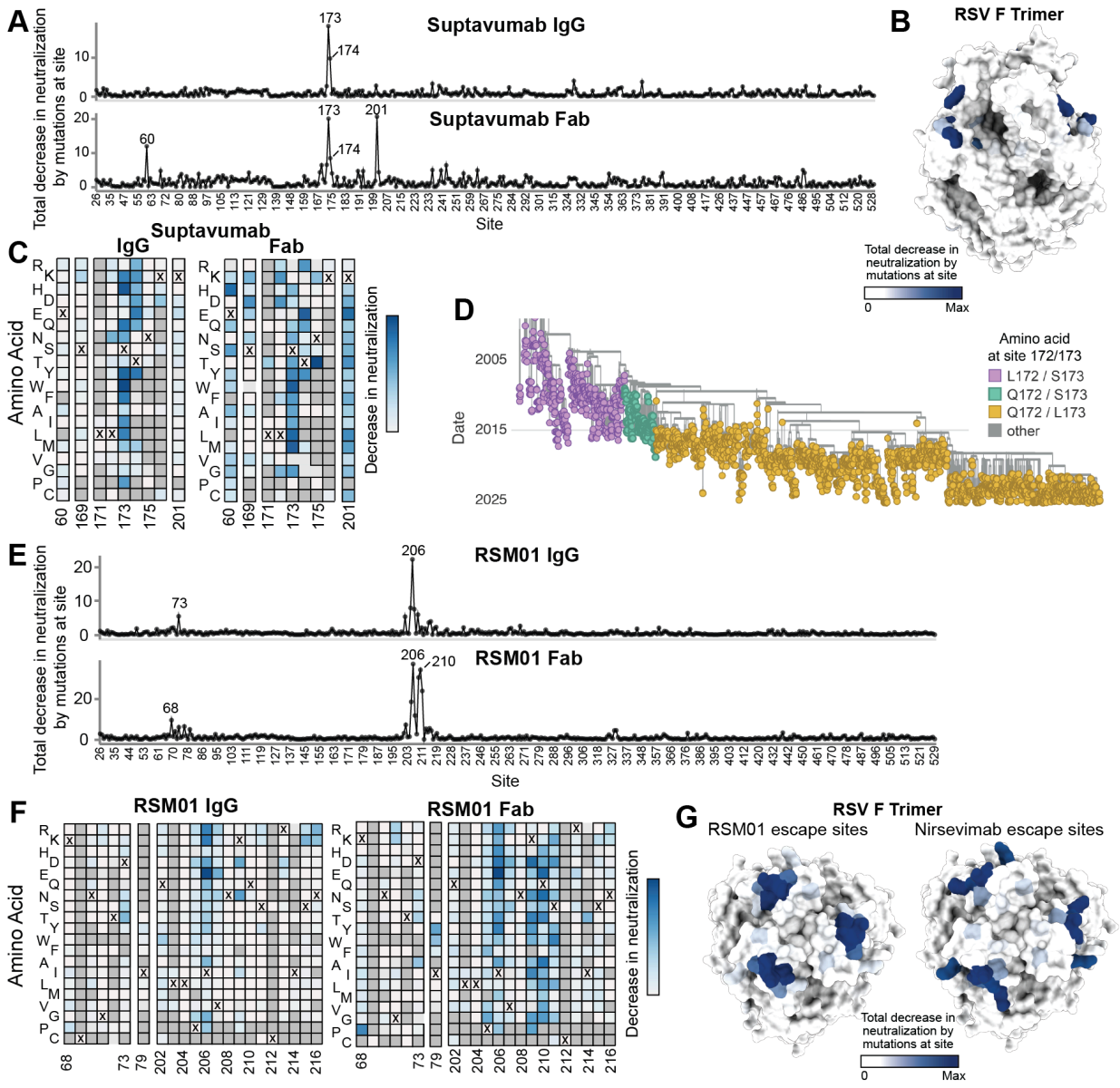

Figure 6. Effects of mutations to RSV F on neutralization by suptavumab and RSM01

(A) Total decrease in neutralization from all mutations at each site for suptavumab IgG or Fab as measured by deep mutational scanning. See https://dms-vep.org/RSV_Long_F_DMS/suptavumab_neutralization.html for interactive plots that show the effects of all mutations. **(B)** Heatmaps showing effects on suptavumab neutralization of mutations at top escape sites. Each box represents the effect of a single mutation, with positive values indicating decreased neutralization. Dark gray indicates

bioRxiv preprint doi: https://doi.org/10.64898/2026.02.12.705519; this version posted February 12, 2026. The copyright holder for this preprint (which was not certified by peer review) is the author/funder, who has granted bioRxiv a license to display the preprint in perpetuity. It is made available under aCC-BY 4.0 International license.

mutations that are too deleterious for cell entry to measure their effect on neutralization. Light gray shading indicates mutations that were not measured. The wildtype amino acid in the subtype A Long strain used for the deep mutational scanning at each site is indicated with an 'x'. **(C)** Pre-fusion RSV F trimer (PDB 5UDC[21]) colored by the total effect of mutations at each site on neutralization by suptavumab Fab. **(D)** Phylogenetic trees of subtype B RSV F sequences colored by amino acid identities at sites 172 and 173. **(E)** Total decrease in neutralization from all mutations at each site for RSM01 IgG or Fab as measured by deep mutational scanning. See https://dms-vep.org/RSV_Long_F_DMS/RSM01_neutralization.html for interactive plots that show the effects of all mutations. **(F)** Heatmaps showing effects on RSM01 neutralization of mutations at top escape sites. **(G)** Pre-fusion RSV F trimer (PDB 5UDC[21]) colored by the total effect of mutations at each site on neutralization by RSM01 Fab or nirsevimab Fab.

bioRxiv preprint doi: https://doi.org/10.64898/2026.02.12.705519; this version posted February 12, 2026. The copyright holder for this preprint (which was not certified by peer review) is the author/funder, who has granted bioRxiv a license to display the preprint in perpetuity. It is made available under aCC-BY 4.0 International license.

Supplemental Figures

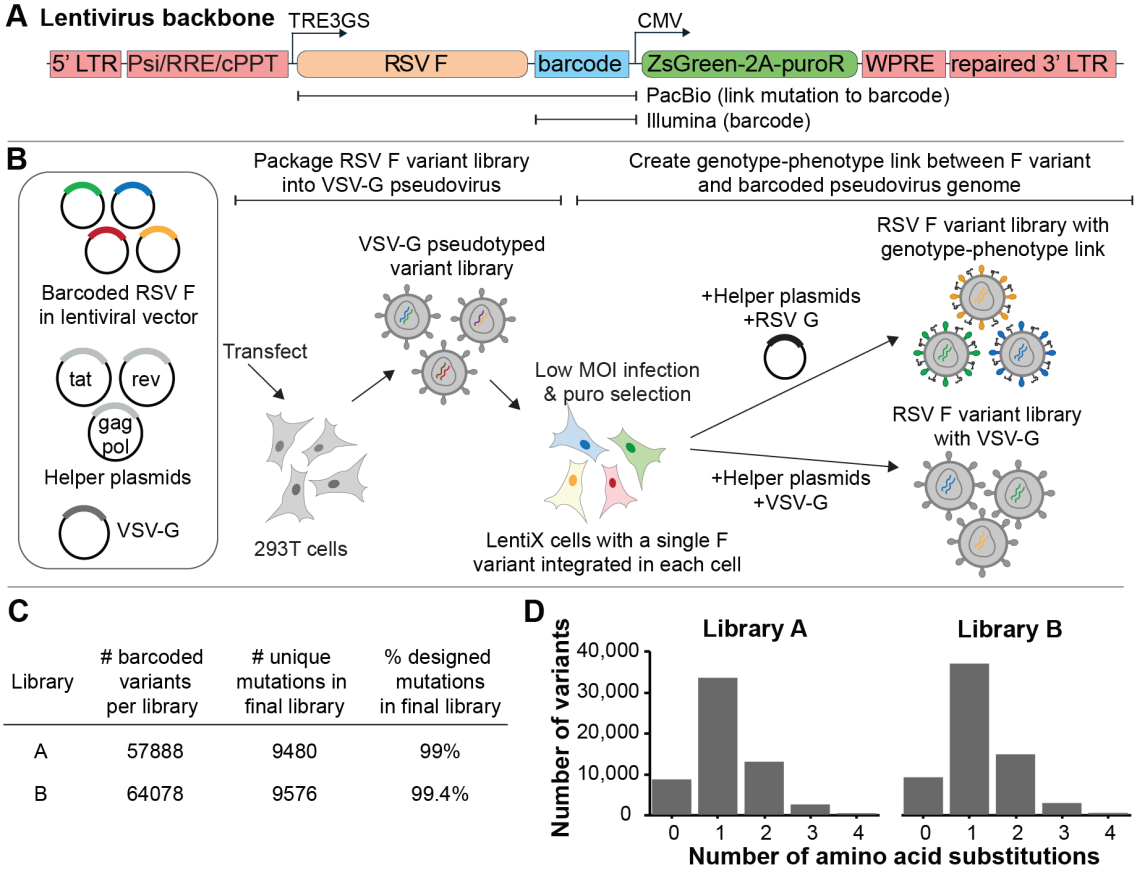

Library	# barcoded variants per library	# unique mutations in final library	% designed mutations in final library
A	57888	9480	99%
B	64078	9576	99.4%

Supplemental Figure 1. Overview of RSV F deep mutational scanning.

(A) Lentivirus genome used to make genotype-phenotype linked pseudovirus libraries. Long-read PacBio sequencing is used to link each barcode to a F mutant. Short-read Illumina sequencing is used to quantify the frequency of F variants in experiments. **(B)** Process to generate pseudovirus libraries. We produce VSV-G-pseudotyped lentiviral particles encoding F in their genomes. LentiX cells are transduced by these particles at low MOI so most infected cells receive only one genome integration. Cells with integrated proviruses are selected using puromycin. The library of F-pseudotyped particles is produced by transfecting lentiviral helper plasmids and RSV G. VSV-G pseudovirus is produced as a control to measure library composition independent of F function. PacBio sequencing is performed after integration into cells to account for lentiviral recombination. **(C)** Number of barcoded variants, number of unique F amino-acid mutations represented at least once among these variants, and percent of all possible F ectodomain mutations in each of the two pseudovirus libraries. **(D)** Distribution of number of mutations per F variant.

bioRxiv preprint doi: https://doi.org/10.64898/2026.02.12.705519; this version posted February 12, 2026. The copyright holder for this preprint (which was not certified by peer review) is the author/funder, who has granted bioRxiv a license to display the preprint in perpetuity. It is made available under aCC-BY 4.0 International license.

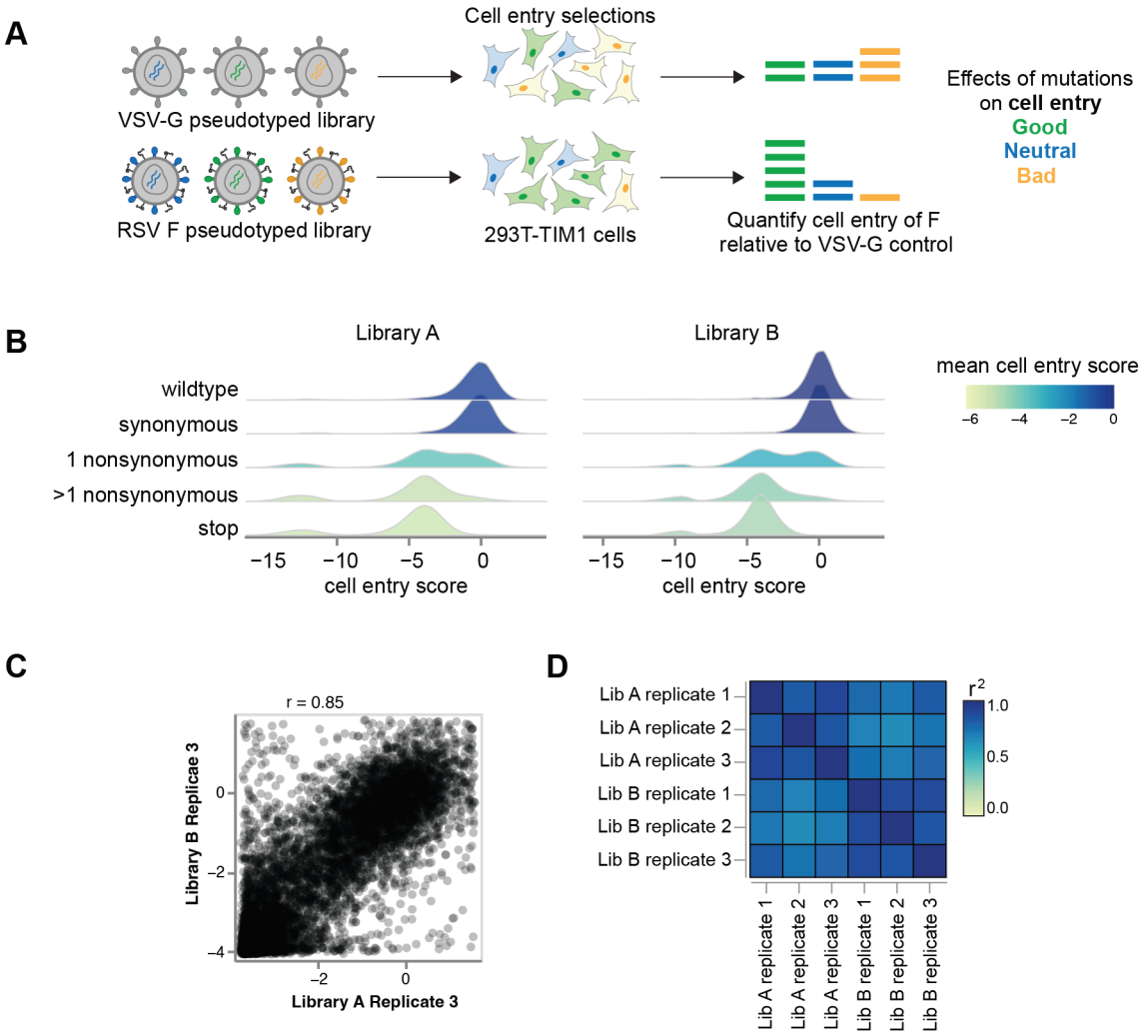

Supplemental Figure 2. Measurement of how mutations affect F-mediated cell entry.

(A) Workflow for measuring effects of mutations on cell entry. Pseudovirus libraries expressing RSV F and G or VSV-G are used to infect 293T-TIM1 cells. After infection, lentivirus genomes are isolated from infected cells and barcodes are sequenced to quantify the ability of each F variant to infect cells. Cell entry is quantified as the log2 ratio of the counts of the barcode in the F-mediated entry versus VSV-G control experiments after normalizing these counts to those for the unmutated F protein. So negative values indicate impaired entry and values of zero indicate no effect. **(B)** Distributions of cell entry scores for the two replicate libraries. Histograms are separated by the type of codon mutation in the mutant. **(C)** Correlation of the effect of mutations on cell entry between a single experimental measurement made using each of the two independent libraries. **(D)** Three experimental replicates were done for each of the two libraries. Correlations of the effects of mutations are shown for each pair of replicates.

bioRxiv preprint doi: https://doi.org/10.64898/2026.02.12.705519; this version posted February 12, 2026. The copyright holder for this preprint (which was not certified by peer review) is the author/funder, who has granted bioRxiv a license to display the preprint in perpetuity. It is made available under aCC-BY 4.0 International license.

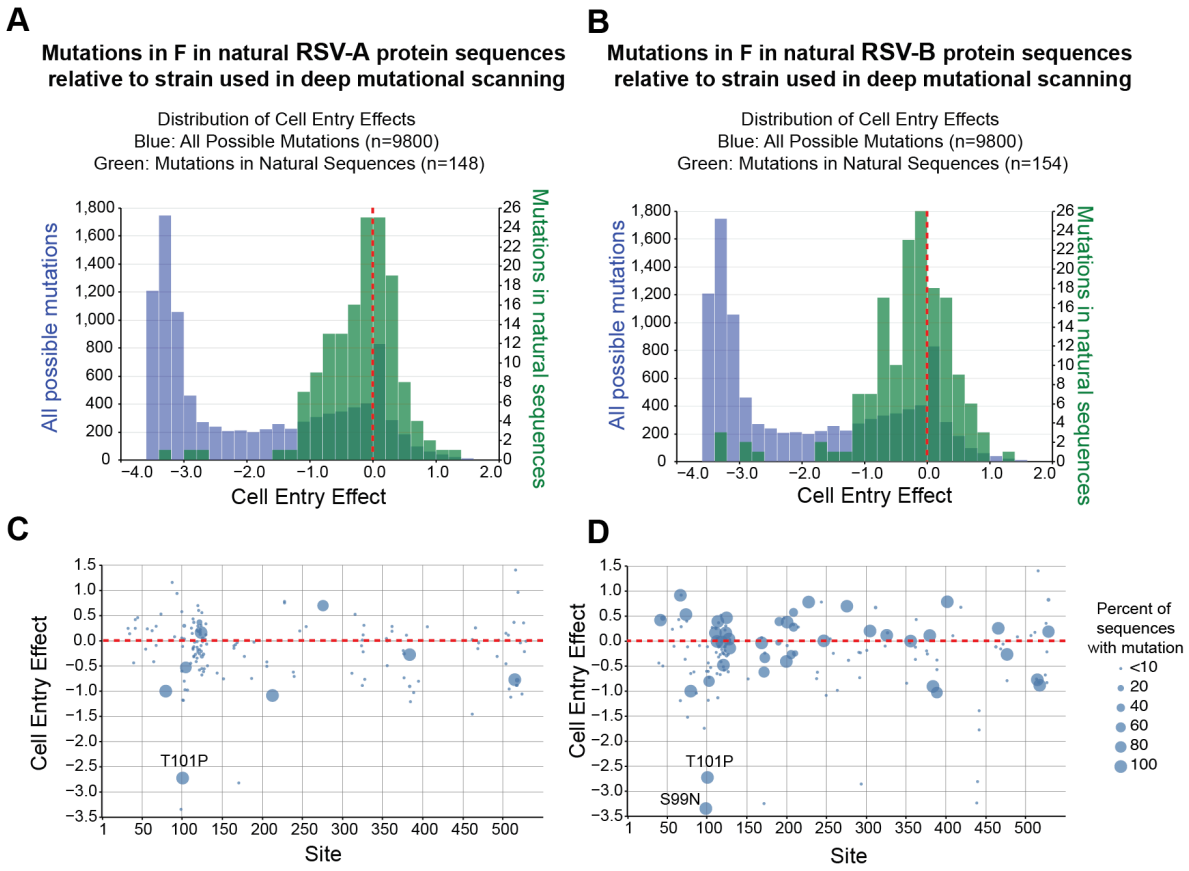

Supplemental Figure 3. Amino acid differences in natural RSV sequences relative to the strain used for deep mutational scanning mostly have minimal impact on cell entry.

(A,B) Distribution of effects on cell entry (as measured by deep mutational scanning) for all possible F protein mutations (blue) and mutations observed in natural RSV F sequences (green) for subtypes A and B. Mutations are defined relative to the lab-adapted subtype A Long strain used in the deep mutational scanning. The red vertical dashed line indicates an effect of zero, corresponding to no impact on cell entry. **(C,D)** Cell entry effects for mutations in natural subtype A and B F sequences relative to the strain used in deep mutational scanning. Each circle represents a mutation, with its x-axis location indicating the site in the protein and its size indicating the percent of F sequences with that mutation. The red dashed line indicates zero effect (neutral). Only two mutations measured to be deleterious to cell entry are at high frequency in natural sequences, T101P and S99N. T101P is found in nearly all natural sequences and S99N is found in nearly all natural subtype B sequences. S99N is likely deleterious in the lab-adapted strain as it creates an N-linked glycosylation site near the F cleavage site. However, this glycosylation site is not formed in natural sequences due to no S/T residues at site 101. T101P is a determinant of human metapneumovirus growth in cell culture[82], suggesting the difference between the lab-adapted strain and natural sequences may be a lab-adaptation.

bioRxiv preprint doi: https://doi.org/10.64898/2026.02.12.705519; this version posted February 12, 2026. The copyright holder for this preprint (which was not certified by peer review) is the author/funder, who has granted bioRxiv a license to display the preprint in perpetuity. It is made available under aCC-BY 4.0 International license.

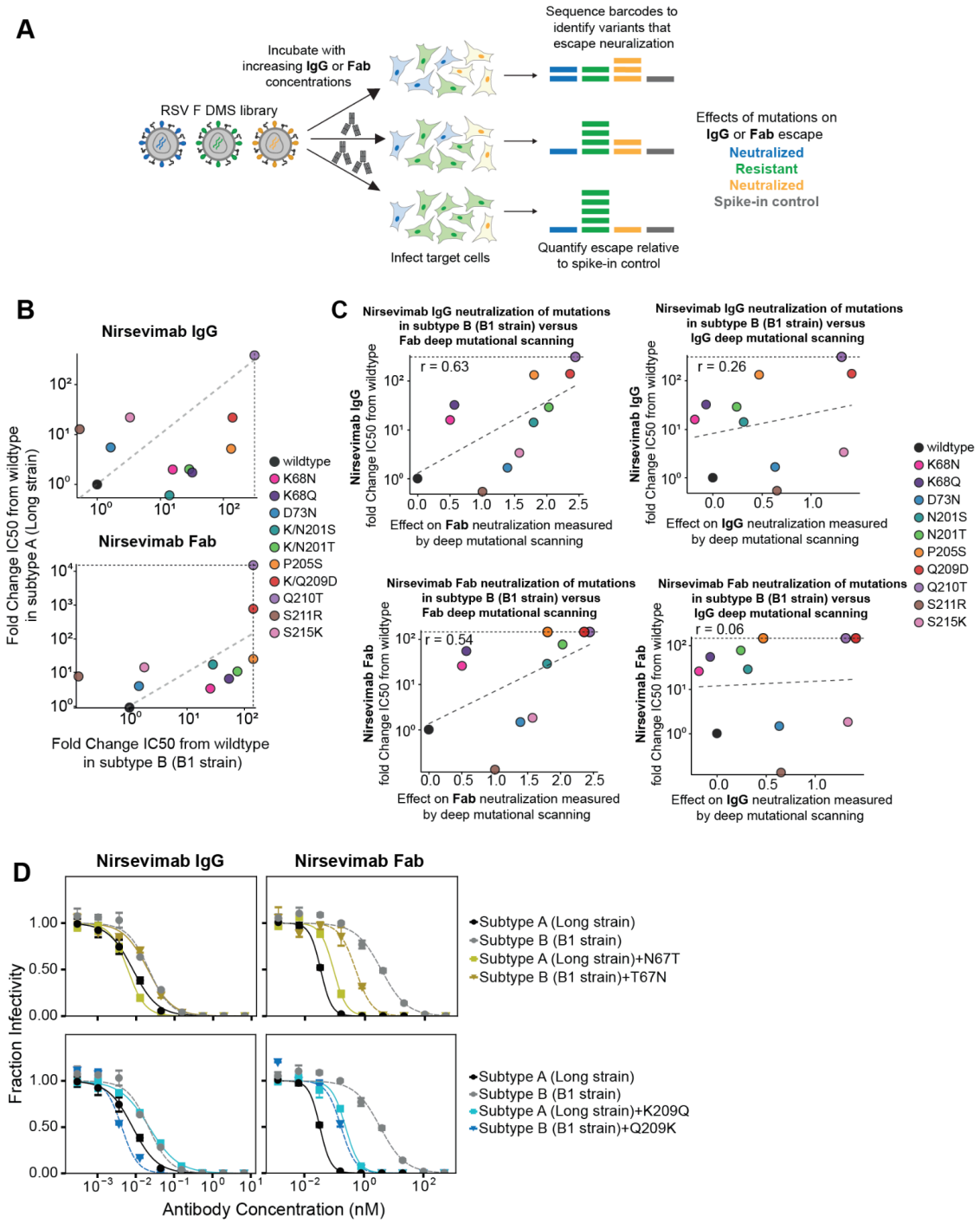

Supplemental Figure 4. Deep mutational scanning measurements versus effects of mutations on subtype B as measured in validation neutralization assays.

(A) Workflow for measuring effects of mutations on antibody neutralization using deep mutational scanning. Pseudovirus libraries expressing RSV F and G are used to infect

bioRxiv preprint doi: https://doi.org/10.64898/2026.02.12.705519; this version posted February 12, 2026. The copyright holder for this preprint (which was not certified by peer review) is the author/funder, who has granted bioRxiv a license to display the preprint in perpetuity. It is made available under aCC-BY 4.0 International license.

293T-TIM1 cells after incubation with increasing concentrations of antibody (IgG or Fab). After infection, lentivirus genomes are isolated from infected cells and combined with equal amounts of a DNA spike-in standard containing known barcodes. The barcodes are sequenced to quantify the ability of each F variant to infect cells in each antibody concentration, with barcode sequencing counts converted to fraction infectivity by normalizing them to the counts for the spike-in standard (see Methods). Details including all data for experimental replicates are shown here https://github.com/dms-vep/RSV_Long_F_DMS. **(B)** Correlation between effects of mutations on neutralization IC50 of subtype A (Long strain) or subtype B (B1 strain) F pseudoviruses in validation neutralization assays with nirsevimab IgG and Fab. Dashed gray line shows 1:1. **(C)** Correlation between effects of mutations in the deep mutational scanning of subtype A F with nirsevimab Fab or IgG versus effects on IC50 in validation neutralization assays using a subtype B (B1 strain) F. As predicted by the biophysical model, deep mutational scanning with the Fab is more predictive of effects of mutations in subtype B. Horizontal and vertical dashed lines indicate limits of detection. **(D)** Differences between subtype A and B at F sites 67 and 209 contribute to reduced potency of nirsevimab against subtype B. These neutralization curves are duplicated from Figure 3, and the same curves for the unmutated subtype A (Long strain) and subtype B (B1 strain) are plotted in both the top and bottom rows.

bioRxiv preprint doi: https://doi.org/10.64898/2026.02.12.705519; this version posted February 12, 2026. The copyright holder for this preprint (which was not certified by peer review) is the author/funder, who has granted bioRxiv a license to display the preprint in perpetuity. It is made available under aCC-BY 4.0 International license.

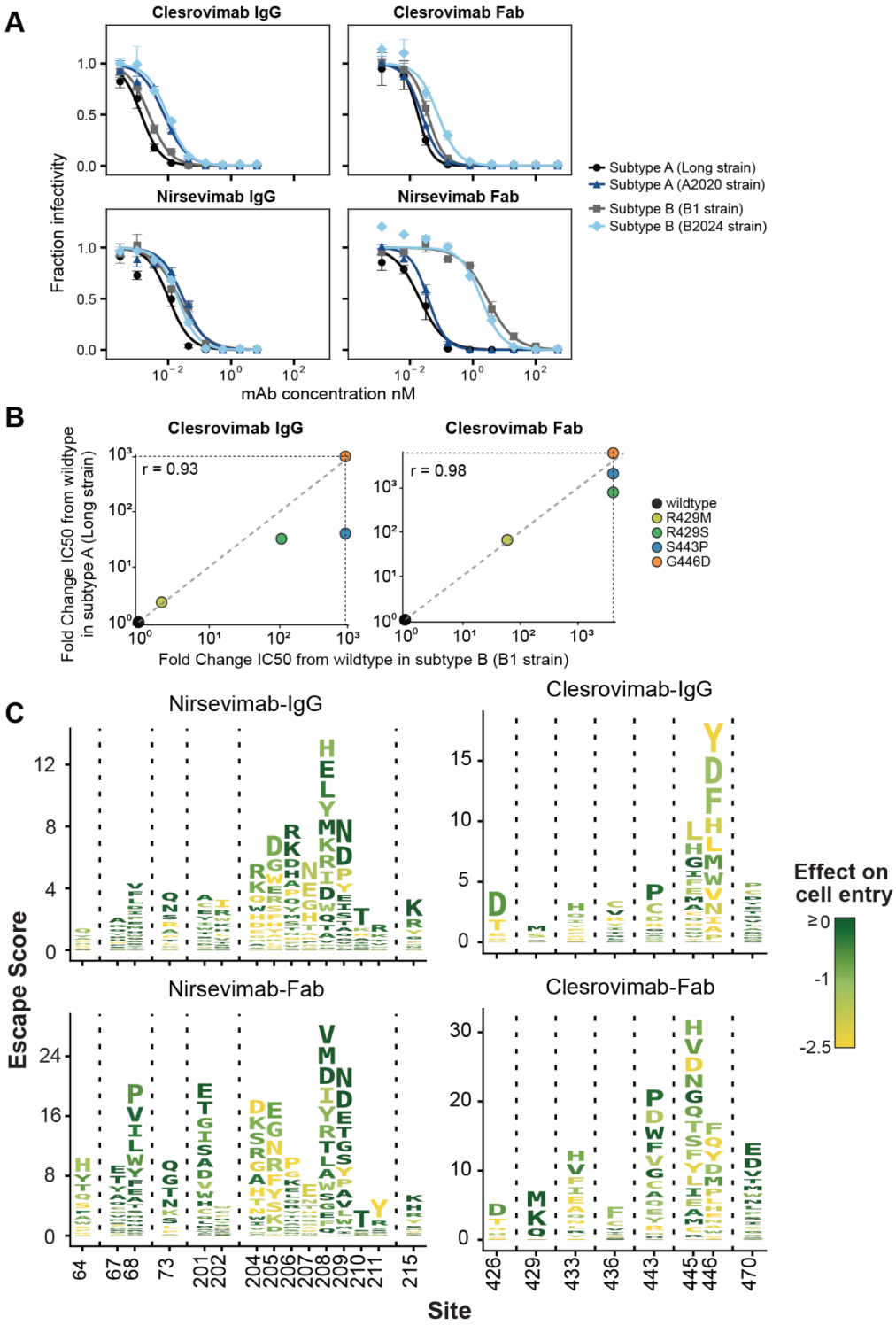

Supplemental Figure 5. Mutations that affect clesrovimab neutralization have similar effects in subtypes A and B.

(A) Neutralization curves for both the IgG and Fab forms of clesrovimab and nirsevimab IgG and Fab against pseudoviruses with F from two subtype A strains (the lab-adapted Long strain

bioRxiv preprint doi: https://doi.org/10.64898/2026.02.12.705519; this version posted February 12, 2026. The copyright holder for this preprint (which was not certified by peer review) is the author/funder, who has granted bioRxiv a license to display the preprint in perpetuity. It is made available under aCC-BY 4.0 International license.

and the recent clinical strain A2020) and two subtype B strains (the lab-adapted B1 strain and the recent clinical B2024 strain). **(B)** Correlation between effects of mutations on neutralization IC50 of subtype A (Long strain) or subtype B (B1 strain) F pseudoviruses in validation neutralization assays with clesrovimab IgG and Fab. Dashed gray line shows 1:1.
(C) Mutations that reduce clesrovimab neutralization tend to be more deleterious for F's cell entry function than mutations that reduce nirsevimab neutralization. Logo plots showing the effects of mutations at key sites on neutralization by nirsevimab or clesrovimab, measured by deep mutational scanning using IgG or Fab. The height of each letter is proportional to the reduction in neutralization mutation to that amino acid causes in the deep mutational scanning. Mutations are colored by their effect on F-mediated cell entry in the absence of antibody as measured by deep mutational scanning, with dark green indicating no effect on cell entry and yellow indicating reduced cell entry. Therefore, yellow letters represent mutations that are likely to be deleterious to viral fitness even if they reduce antibody neutralization. Note that it is impossible to measure the effect on neutralization of mutations that fully ablate cell entry, so these plots only show mutations that retain at least some moderate level of cell entry (a cell entry effect > -2.5 in our measurements). See (Figure 2 and associated hyperlinks to interactive plots) for data on how all mutations at sites in the nirsevimab and clesrovimab epitopes affect cell entry function.

bioRxiv preprint doi: https://doi.org/10.64898/2026.02.12.705519; this version posted February 12, 2026. The copyright holder for this preprint (which was not certified by peer review) is the author/funder, who has granted bioRxiv a license to display the preprint in perpetuity. It is made available under aCC-BY 4.0 International license.

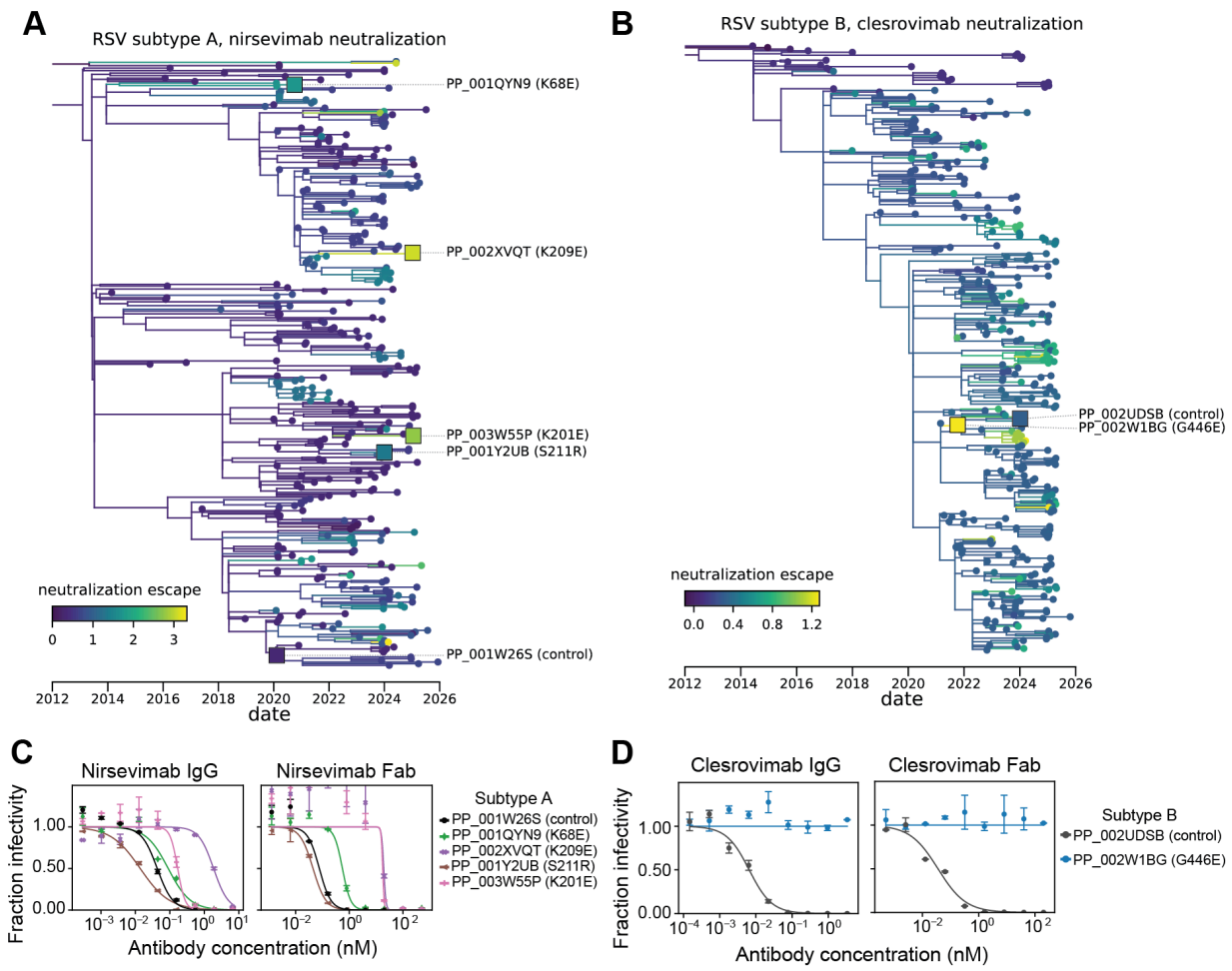

Supplemental Figure 6. Additional phylogenetic trees and validation assays showing sporadic nirsevimab and clesrovimab resistance mutations in natural RSV sequences.

This figure is like Figure 5 except it shows **(A)** trees of subtype A RSV F with nirsevimab escape scores, **(B)** trees of subtype B RSV F with clesrovimab escape scores, **(C)** neutralization assays validating reduced neutralization of natural subtype A strains by nirsevimab, and **(D)** neutralization assays validating reduced neutralization of a natural subtype B strain by clesrovimab. Note that that subtype A strain PP_001Y2UB strain does not have reduced nirsevimab neutralization despite a high escape score driven the S211R resistance mutation (which Figure 3D validates reduces nirsevimab neutralization in another subtype A strain); we speculate that neutralization of strain PP_001Y2UB might be affected by an epistatic interaction between S211R and a second R213S mutation it contains at a nearby site.

bioRxiv preprint doi: https://doi.org/10.64898/2026.02.12.705519; this version posted February 12, 2026. The copyright holder for this preprint (which was not certified by peer review) is the author/funder, who has granted bioRxiv a license to display the preprint in perpetuity. It is made available under aCC-BY 4.0 International license.

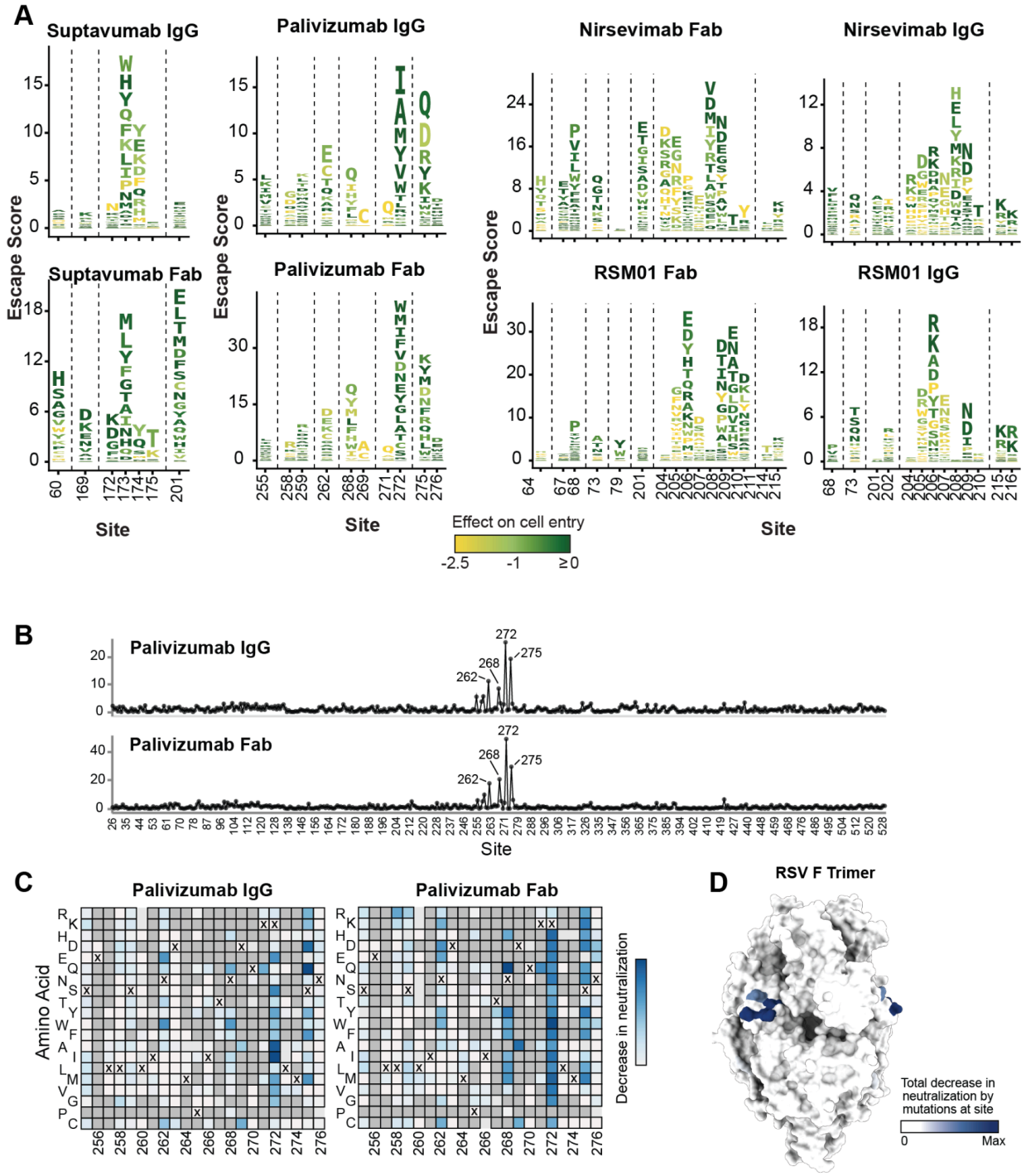

Supplemental Figure 7. Effects of F mutations on neutralization by suptavumab, palivizumab and RSM01

(A) Logo plots showing the effects of mutations at key sites on neutralization by suptavumab, palivizumab, nirsevimab and RSM01, measured by deep mutational scanning using IgG or Fab.

bioRxiv preprint doi: https://doi.org/10.64898/2026.02.12.705519; this version posted February 12, 2026. The copyright holder for this preprint (which was not certified by peer review) is the author/funder, who has granted bioRxiv a license to display the preprint in perpetuity. It is made available under aCC-BY 4.0 International license.

The height of each letter is proportional to the reduction in neutralization a mutation to that amino acid causes in the deep mutational scanning. Mutations are colored by their effect on F-mediated cell entry in the absence of antibody as measured by deep mutational scanning, with dark green indicating no effect on cell entry and yellow indicating reduced cell entry. Therefore, yellow letters represent mutations that are likely to be deleterious to viral fitness even if they reduce antibody neutralization. It is impossible to measure the effect on neutralization of mutations that fully ablate cell entry, so these plots only show mutations that retain at least some moderate level of cell entry (a cell entry effect > -2.5 in our measurements). Logo plots for nirsevimab are also shown in Supplemental Figure 7, but are shown again here to facilitate comparison between nirsevimab and RSM01. **(B)** Total decrease in neutralization from all mutations at each site for palivizumab IgG or Fab as measured by deep mutational scanning. See https://dms-vep.org/RSV_Long_F_DMS/palivizumab_neutralization.html for interactive plots that show the effects of all mutations. **(C)** Heatmaps showing effects on neutralization of mutations at top escape sites. Each box represents the effect of a single mutation, with positive values indicating decreased neutralization. Dark gray indicates mutations that are too deleterious for cell entry to measure their effect on neutralization. Light gray shading indicates mutations that were not measured. The wildtype amino acid in the subtype A Long strain used for the deep mutational scanning at each site is indicated with an 'x'. **(D)** Pre-fusion RSV F trimer (PDB 5UDC[21]) colored by the total effect of mutations at each site on neutralization by palivizumab Fab.

bioRxiv preprint doi: https://doi.org/10.64898/2026.02.12.705519; this version posted February 12, 2026. The copyright holder for this preprint (which was not certified by peer review) is the author/funder, who has granted bioRxiv a license to display the preprint in perpetuity. It is made available under aCC-BY 4.0 International license.

Methods

Data availability

All data and interactive figures are publicly available:

- Homepage for exploring interactive visualizations of deep mutational scanning data: https://dms-vep.org/RSV_Long_F_DMS/
- GitHub repository of all code used to analyze and visualize deep mutational scanning data, as well as processed data giving all sequencing counts and inferred mutation effects: https://github.com/dms-vep/RSV_Long_F_DMS
- Final measured effects of mutations on cell entry and antibody neutralization after data QC: https://github.com/dms-vep/RSV_Long_F_DMS/blob/main/results/summaries/all_antibodies.csv

Biosafety

We performed all experiments with pseudotyped lentiviral particles at biosafety level 2[83]. These pseudoviruses do not encode any other viral proteins other than RSV F and therefore can only undergo a single round of cell entry and are not fully replicative infectious agents capable of causing disease. The other viral proteins needed for the formation of pseudotyped lentiviral particles (RSV G, and the lentiviral Gag/Pol, Tat, and Rev) were provided during pseudovirus production by transfection of four separate helper plasmids and are not encoded in the viral genome. Therefore, this study did not generate any mutants of actual replicative human pathogenic virus.

Antibodies

The RSV monoclonal antibodies nirsevimab[21,33], clesrovimab[22,62], palizumab[69], suptavumab[26] and RSM01[16] were produced by Genscript as human IgG1 kappa isotypes and Fabs. Sequences were obtained from the referenced publications, structures in the Protein Data Bank or original patents. Palivizumab originated from patent US6955717B2. See Simonich et al. 2025 for antibody amino acid sequences[55]. The sequence of RSM01 was shared by the Gates Medical Research Institute.

Plasmids and primers

All plasmid and primer sequences used in this study can be found here (https://github.com/dms-vep/RSV_Long_F_DMS/tree/main/supplemental_data). All primers were ordered from Integrated DNA Technologies.

Cell line handling

All cell lines (293T, 293T-TIM1[55] and Takara Lenti-X™ 293T) were cultured in D10 media (Dulbecco's Modified Eagle Medium supplemented with 10% heat-inactivated fetal bovine serum, 2 mM l-glutamine, 100 U/mL penicillin, and 100 mg/mL streptomycin) and cultured at 37ºC with 5% CO2.

Design of deep mutational scanning libraries of RSV F

We created pseudovirus libraries containing nearly all possible single amino-acid mutations to the ectodomain of the RSV F protein. We used unmutated parental F from the Long strain of RSV, which is a subtype A, lab-adapted strain isolated in the 1950s[56]. We codon optimized this sequence using the GenSmart codon optimization tool offered by GenScript and removed four amino acids from the cytoplasmic tail to increase pseudovirus titers[55]. We used a lentiviral backbone that contains an extended Gag sequence to enhance packaging of lentiviral genomes as previously described[84,85]. The plasmid map for the lentiviral backbone with codon-optimized RSV F sequence is at:

bioRxiv preprint doi: https://doi.org/10.64898/2026.02.12.705519; this version posted February 12, 2026. The copyright holder for this preprint (which was not certified by peer review) is the author/funder, who has granted bioRxiv a license to display the preprint in perpetuity. It is made available under aCC-BY 4.0 International license.

https://github.com/dms-vep/RSV_Long_F_DMS/blob/main/supplemental_data/plasmids/4821_v5lp_phru3_forind-extgag_RSV_Long_F_GS4Opt_4aaCTdel.gb.

We aimed to include all single amino acid mutations in the RSV F ectodomain (residues 26-529; 504 x 19 = 9576 mutations). We also included 30 stop codons located at alternating positions from the start of the ectodomain as a negative control for cell entry measurements. We ordered a site-saturation variant library with these criteria from Twist Biosciences. The final Twist quality control report for the library is at: https://github.com/dms-vep/RSV_Long_F_DMS/blob/main/supplemental_data/Final_QC_Report_Q-392996_VariantProportion.csv.

Cloning of deep mutational scanning plasmid libraries of RSV F

The RSV F library was designed to have all mutations to the ectodomain of F. However, 268 mutations were missing from the library produced by Twist. We added the missing mutations and also over-represented mutations in the nirsevimab binding site (amino acid residues 62-29 and 196-212) because we wanted to ensure inclusion and measurement of effects of all possible mutations in the epitope. We aimed to clone a "spike-in" plasmid library that contains these missing mutations and over-representation of mutations in the nirsevimab binding site using a mutagenesis PCR protocol[86–88]. We designed NNS primers for the nirsevimab-targeting sites with with https://github.com/jbloomlab/CodonTilingPrimers and primers for missing mutations with https://github.com/jbloomlab/TargetedTilingPrimers. Forward and reverse primer pools were created by combining either forward or reverse NNS and targeted mutation primers at an equal molar ratio per codon for a final concentration of 5µM. Linear template of RSV F was made by digesting the lentiviral backbone with codon-optimized RSV F sequence with NotI-HF and NdeI. PCR mutagenesis was then performed as described previously[54] with the only difference being that 7 PCR cycles were used for the mutagenesis PCR to reduce the resulting number of multi-mutants. After the PCR, the product was digested using DpnI for 20 minutes at 37°C to remove any leftover template. The PCR mutagenesis to generate the "spike-in" was performed in duplicate, once for library A and once for library B.

We then barcoded the library pools made by Twist Biosciences independently in two separate reactions to make library A and B respectively. These two biological replicates were handled separately for all subsequent experimental steps. The barcoding was performed as in Dadonaite et al.[54] using primers containing a random 16 nucleotide sequence downstream of the RSV F stop codon. The only difference from Dadonaite et al. is that only 5 ng of template was used. The two pools of mutagenized RSV F for the "spike-in" were also barcoded separately. In all there were four separate barcoding PCR reactions. The lentiviral backbone (4016_V5LP_pHrU3_ForInd-Extgag_mcherry)[85] was digested with MluI-HF and XbaI at 37°C for 45 minutes then gel purified and purified using AMPure XP beads (Beckman Coulter Cat #A63881). The barcoded libraries were cloned into the lentiviral backbone at a 1:2 insert to vector ratio in a HiFi assembly for 1 hour at 50°C. The HiFi product was purified with AMPure XP beads and eluted in molecular grade water. The purified products were transformed into 10-beta electrocompetent cells (New England Biolabs Cat #C3020K) using a BioRad MicroPulser Electroporator, shocking at 2 kV for 5 milliseconds. 10 reactions of electroporation were performed per barcoded Twist library and 2 reactions per mutagenized spike-in library. Following the 1 hour recovery at 37°C, transformed cells were spun out of SOC and pooled and cultured in 150 mL LB medium for each Twist library and 100 mL LB medium for each spike-in library with ampicillin overnight at 37°C in a shaking incubator. Plasmids were extracted using the QIAGEN HiSpeed Plasmid Maxi Kit (QIAGEN Cat #12662).

Corresponding replicates of the Twist plasmid libraries and spike-in plasmid libraries were combined at a 1:1.25 Twist to spike-in molar ratio per codon because long-read PacBio sequencing of the

bioRxiv preprint doi: https://doi.org/10.64898/2026.02.12.705519; this version posted February 12, 2026. The copyright holder for this preprint (which was not certified by peer review) is the author/funder, who has granted bioRxiv a license to display the preprint in perpetuity. It is made available under aCC-BY 4.0 International license.

plasmid libraries revealed this ratio results in the most even distribution of mutants in the combined libraries.

Production of cell-stored deep mutational scanning libraries

Cells storing the deep mutational scanning libraries as single integrated RSV F containing genomes per cell were produced as described in prior work[54] with a few changes (Supplemental Figure 1B). VSV-G pseudotyped lentiviruses were produced by transfecting four 10 cm dishes of 293T cells with the lentiviral backbone containing the barcoded RSV F libraries per library (5 μg per dish), lentiviral Gag/Pol, Tat, and Rev helper plasmids (1.25 ug per dish, AddGene: HDM-tat1b product ID 204154, pRC-CMV-Rev1b product ID 20413, HDM-Hgpm2 product ID 204152)[54] and a VSV-G expression plasmid (1.25 ug per dish, AddGene pMD2.G product ID 12259) using BioT (Bioland Scientific, Cat #B01-02).

While previous deep mutational scanning studies have integrated into a specific clone of 293T-rtTA cells that were previously found to yield good pseudovirus titers for other viral entry proteins[54], we found that this clone was unable to generate high titer RSV pseudovirus. We tested multiple clones of 293T-rtTA cells but found that the highest titer RSV pseudovirus produced from singly integrated cells was produced from Takara's Lenti-X™ 293T Cell Line (Cat #632180). This clonal 293T cell line does not overexpress rtTA. Our lentiviral backbone includes a dox-inducible promoter; in other deep mutational scanning studies which use 293T-rtTA cells and a similar backbone, dox is added to induce expression from the lentiviral backbone[54]. We found that for production from RSV F cell stored libraries, pseudovirus titers were sufficiently high when expression was induced only from Tat at transfection. We found no additional benefit with transfection of rtTA and addition of doxycycline when producing pseudovirus. Therefore, we used Takara's Lenti-X™ 293T Cell Line for the cell stored library. To make the cell stored library, the VSV-G pseudotyped viruses were used to infect Takara's Lenti-X™ 293T Cell Line at an infection rate of <1% so that most transduced cells would receive only a single integrated genome. Transduced cells were selected using puromycin so that the final population of cells contained an integrated genome encoding a single barcoded variant of RSV F. These cells were expanded and frozen with at least 2e7 cells per aliquot and stored in liquid nitrogen for later use.

Rescue of F and VSV-G expressing pseudovirus libraries

To rescue F expressing pseudoviruses from the integrated cells, 100 million cells were plated in 5-layer flasks. The following day, each flask was transfected with 118.75 ug of each helper plasmid (AddGene: HDM-tat1b product ID 204154, pRC-CMV-Rev1b product ID 20413, HDM-Hgpm2 product ID 204152) and 18.75 ug of RSV G expression plasmid (AddGene: HDM_RSV_Long_G_31AACTdel Product ID 237350). Xfect transfection reagent (Cat #631318) was used according to the manufacturer's instructions (112.5uL Xfect transfection reagent and 7.5 mL buffer per 5-layer flask). At 48 hours post transfection, the supernatant was filtered through a 0.45um SFCA Nalgene 500 mL Rapid-Flow filter unit (Cat #09-740-44B). Filtered supernatant was then concentrated by ultracentrifugation with a 20% sucrose cushion in HBSS (Fisher Cat# 14025092) at 100,000 g for 1 h at >20ºC. The pseudoviruses pelleted to the bottom of the cushion, after disposal of the supernatant, pellets were resuspended in D10. Aliquots of concentrated F-expressing pseudoviruses were flash frozen as previously described[55] and stored at -80°C for use in downstream selection experiments.

To rescue VSV-G expressing pseudoviruses from integrated cells, 100 million cells were plated in 5-layer flasks. The following day, each flask was transfected with 37.5 ug each helper (AddGene: HDM-tat1b product ID 204154, pRC-CMV-Rev1b product ID 20413, HDM-Hgpm2 product ID 204152) and VSV-G expression plasmid (AddGene pMD2.G product ID 12259). BioT transfection reagent was used according to the manufacturer's instructions. At 48 hours post-transfection, the supernatant was filtered through a 0.45um SFCA Nalgene 500 mL Rapid-Flow filter unit and concentrated using LentiX

bioRxiv preprint doi: https://doi.org/10.64898/2026.02.12.705519; this version posted February 12, 2026. The copyright holder for this preprint (which was not certified by peer review) is the author/funder, who has granted bioRxiv a license to display the preprint in perpetuity. It is made available under aCC-BY 4.0 International license.

concentrator (Takara, Cat #631232) at a 1:3 virus to concentrator ratio, incubating at 4°C for 3 hours and spinning at 1500 x g and 4°C for 45 minutes. Following centrifugation, supernatant was discarded and viral pellets resuspended in D10. Aliquots of concentrated VSV-G expressing pseudoviruses were frozen at -80°C for later use.

Long-read PacBio sequencing for variant-barcode linkage

To link the barcode sequences with the mutations found in RSV F we used long-read PacBio sequencing of the lentiviral genomes in pseudoviruses made from the cell stored libraries. We performed PacBio barcode-mutation linking after generating the singly integrated cell libraries because template switching of the pseudodiploid lentiviral genome during reverse transcription can alter barcode-variant pairings relative to the original plasmid pool. Sequencing the integrated library ensures that barcode-variant linkages reflect those present in the actual integrated provirus. This process has been described previously[54]. For this library we made a few alterations. 1e6 293T-TIM1 cells were plated in each well of 6-well plates coated with poly-L-lysine. The next day, 30 million TU's of VSV-G expressing library pseudoviruses were used to infect cells (6 wells for each library at 5 million TU/well). At 12 hours post-infection, the non-integrated reverse-transcribed lentiviral genomes were recovered by miniprepping the 293T-TIM1 cells as described in prior work[54]. Amplicons for long-read sequencing of the miniprepped genomes were prepared by following a previously described approach[54,88]. The PCR reactions for each library were combined and amplicon length was verified by TapeStation prior to sequencing. Libraries were each sequenced on a single SMRT cell with a movie length of 30 hours on a PacBio Sequel IIe sequencer. To maximize identification of all variants present, each library was sequenced a second time.

We used the *dms-vep-pipeline-3* package (https://github.com/dms-vep/dms-vep-pipeline-3), to process sequencing data. To link specific mutations with each barcode, PacBio circular consensus sequences were aligned to the unmutated RSV F reference sequence using the *Alignparse* package[89]. Reads were filtered out if they aligned poorly, had a higher than expected number of mutations in the unmutated regions, did not contain a barcode or were the result of strand exchange. Consensus sequences for each barcode/variant sequence were constructed using *alignparse,* while requiring a minimum of three CCS reads and a max cutoff of 0.2 for any minor variants within the consensus. The final barcode/variant lookup tables were used as a reference for all downstream analyses of short-read Illumina sequencing of the barcodes only.

The final barcode-variant table can be found here:
https://github.com/dms-vep/RSV_Long_F_DMS/blob/main/results/variants/codon_variants.csv

For full details on the analysis, see these notebooks for:

- Analyzing the PacBio CCS's:
  https://dms-vep.org/RSV_Long_F_DMS/notebooks/analyze_pacbio_ccs.html
- Building PacBio consensus sequences:
  https://dms-vep.org/RSV_Long_F_DMS/notebooks/build_pacbio_consensus.html
- Building the final barcode-variant table:
  https://dms-vep.org/RSV_Long_F_DMS/notebooks/build_codon_variants.html

The final libraries contained 57,888 and 64,078 unique barcoded variants for LibA and LibB, respectively that covered 99 and 99.4% of all amino-acid mutations (Supplemental Figure 1C). More than half of the variants contain a single amino-acid mutation, with the others having zero or multiple mutations (Supplemental Figure 1D).

bioRxiv preprint doi: https://doi.org/10.64898/2026.02.12.705519; this version posted February 12, 2026. The copyright holder for this preprint (which was not certified by peer review) is the author/funder, who has granted bioRxiv a license to display the preprint in perpetuity. It is made available under aCC-BY 4.0 International license.

Measuring effects of F mutations on cell entry

To measure effects of F mutations on cell entry, we generally followed the approach described in Dadonaite et al.[54] with the following modifications. We infected 293T-TIM1 cells with the pseudovirus libraries displaying the RSV F protein mutants alongside parallel infection of 293T-TIM1 cells with control pseudovirus displaying VSV-G to make their cell-entry independent of RSV F protein function (Supplemental Figure 2A). 2e6 293T-TIM1 cells were plated in each well of 6-well plates coated with poly-L-lysine. The next day, we infected cells with ~12e6 TU total (3e6 TU per well) of F pseudovirus library or ~30e6 TU total (5e6 TU per well) of VSV-G pseudovirus library. After addition of pseudovirus, cells infected with the F pseudovirus library were spun at 900g for 3 hours at 30C. For some selections, 20ug/mL DEAE-dextran was added to the media at the time of infection as this increases pseudovirus titers. However, poor cell health was found to contribute to reduced recovery of infecting barcodes, so DEAE was not used for follow-up selections. At 12 hours post infection, the non-integrated reverse-transcribed lentiviral genomes were recovered by miniprepping the cells. To prepare the amplicons for Illumina sequencing with dual indexing, PCR was performed as described in Yu et al[88]. Samples were pooled in equal DNA amounts and run on a 1% agarose gel. The correct size band was excised, purified with Ampure XP beads, diluted to a concentration of 5 nM, and sequenced on an Illumina NextSeq 2000 (with P3 reagent kit) or NovaSeq X Plus system.

We quantified the effects of mutations as the log2 cell entry of each mutant relative to the unmutated F, using global epistasis models[57,58] to jointly analyze the single and multi-mutant data. Briefly, Illumina sequencing reads were aligned to the barcode variant table generated from the PacBio CCS described above. We next compared the frequency of barcodes between the VSV-G and F_{mutant} selections using the package *dms_variants* (https://github.com/jbloomlab/dms_variants) as previously described[54]. Cell entry scores for each variant were calculated using log enrichment ratio: log_2 ([n^{v}_{post} / n^{wt}_{post}]/[n^{v}_{pre} / n^{wt}_{pre}]), where n^{v}_{post} is the count of variant v in the F-pseudotyped infection (postselection condition), n^{v}_{pre} is the count of variant v in the VSV-G-pseudotyped infection (preselection condition), and n^{wt}_{post} and n^{wt}_{pre} are the counts for wild-type variants. Positive cell entry scores indicate that a variant is better at entering the cells compared to the unmutated parental F, and negative scores indicate entry worse than the parental F. As expected, variants with only synonymous mutations had wildtype-like cell entry scores of zero, variants with stop codon mutations had highly negative scores, and variants with amino-acid mutations had scores ranging from wildtype-like to highly negative (Supplemental Figure 2B). To calculate the mutation-level cell entry effects, a sigmoid global-epistasis function was fitted to variant entry scores after truncating the values at a lower bound of the median functional score of all variants with stop codons, using the *multi-dms* software package. For the mutation effects, values of zero mean no effect on cell entry, negative values mean impaired cell entry, and positive values mean improved cell entry. To generate the final cell entry effect values for each mutation, we performed a total of three technical replicates for each library, for a total of six functional selections (three each from LibA and LibB). The effects for each mutation were then averaged from the six functional selections. To filter out low quality or noisy data, we required each mutation to occur with two unique barcodes and removed any mutation that had a high standard deviation between replicates. The measured cell entry effects were highly correlated both between replicates and libraries (Supplemental Figure 2C-D). The final cell entry effect values reported in the figures correspond to the average effect across libraries and replicates.

Measuring effects of F mutations on antibody neutralization

To measure effects of F mutations on antibody neutralization, we used a previously described method[54] with a few modifications detailed here. 2e6 293T-TIM1 cells were plated in individual wells of poly-L-lysine coated 6-well plates. The next day, ~1.5-2e6 TU of F pseudovirus library were incubated

bioRxiv preprint doi: https://doi.org/10.64898/2026.02.12.705519; this version posted February 12, 2026. The copyright holder for this preprint (which was not certified by peer review) is the author/funder, who has granted bioRxiv a license to display the preprint in perpetuity. It is made available under aCC-BY 4.0 International license.

with D10 media (no antibody control) or antibody for one hour prior to adding to cells. These incubations were performed in a total volume of 2 mL to reduce the possibility of ligand depletion given that these antibodies have very high potency. Antibody concentrations were selected that generally corresponded to a range at which 50% of variants were neutralized, up to 99.5%. During DNA template extraction, we spiked in DNA plasmid containing eight known barcodes that would correspond to ~1% of the reads in the no-antibody control. This DNA plasmid spike-in allowed us to estimate the amount of neutralization each antibody condition had relative to the no antibody control, as previously described (Supplemental Figure 4A)[54,88].

Following Illumina sequencing of the barcodes, the data were analyzed as described previously. Briefly, the fraction infectivity retained at each antibody concentration was calculated from the barcode counts of the DNA standard. Then, the *polyclonal* (https://jbloomlab.github.io/polyclonal/)[90] software was used to fit neutralization curves and estimates of mutation effects on neutralization. We filtered the effects of mutations on antibody neutralization to retain only mutations with at least two unique barcodes, excluded mutations with very low cell entry scores, and excluded mutations that had high standard deviations in their effect on neutralization across replicates. The reported effects of mutations on antibody neutralization are the average across all replicates (always at least two different experimental selections with each of the two independent libraries, LibA and LibB). For example notebooks showing these analyses, see https://dms-vep.org/RSV_Long_F_DMS/notebooks/fit_escape_antibody_escape_RSV-F-LibA-250402-Nir.html (for analysis of an individual selection experiment) and https://dms-vep.org/RSV_Long_F_DMS/notebooks/avg_escape_antibody_escape_Nirsevimab-IgG.html (for average effects across experiments for an antibody).

Validation of cell entry effects using individual pseudoviruses

To validate the effects of mutations on cell entry, we generated a set of plasmids expressing RSV F within a lentiviral backbone that each contained different single F mutations. The parental RSV F amino acid sequence is identical to the unmutated RSV F sequence used in the lentiviral vector described above for deep mutational scanning. We selected mutations spanning a range of entry effects, which included N67I, S215V, S215P, S398L, E87N, and D486N. We transfected them into 293T cells, along with helper plasmids (AddGene: HDM-tat1b product ID 204154, pRC-CMV-Rev1b product ID 20413, HDM-Hgpm2 product ID 204152)[54] and RSV G in an expression plasmid (AddGene: HDM_RSV_Long_G_31AACTdel Product ID237350). 48 hours later, supernatants were filtered through 0.45uM filters to remove cell debris. The pseudoviruses were titrated on 293T-TIM1 cells using flow cytometry to measure TU/mL as previously described[55]. Average titers for two replicates of each pseudovirus were then compared to the average unmutated RSV F titer.

Analysis of cell entry effects of amino acid differences in natural RSV sequences relative to the strain used for deep mutational scanning

An alignment of RSV F protein sequences for subtype A and B were generated on October 27, 2025 from the RSV Nextstrain workflow[67]. We identified amino acid differences relative to the lab-adapted subtype A Long strain used in the deep mutational scanning - for more details see https://github.com/dms-vep/RSV_Long_F_DMS/tree/main/notebooks/sequence_variation. This was used to compare the distribution of cell entry effects for mutations observed in natural sequences to the distribution of cell entry effects for all mutations measured by deep mutational scanning and calculate the percentage of natural sequences with each mutation as shown in Supplemental Figure 3.

bioRxiv preprint doi: https://doi.org/10.64898/2026.02.12.705519; this version posted February 12, 2026. The copyright holder for this preprint (which was not certified by peer review) is the author/funder, who has granted bioRxiv a license to display the preprint in perpetuity. It is made available under aCC-BY 4.0 International license.

Measuring effects of single amino acid mutations on antibody neutralization

We chose previously known and newly identified resistance mutations that had a range of effects on antibody neutralization for nirsevimab and clesrovimab. These mutants were chosen to evaluate the impact of mutations in subtype A and B backgrounds on neutralization by antibody IgG and Fab and to validate the effects of mutations measured by deep mutational scanning on antibody neutralization. The single amino acid mutations were made in a subtype A background (Long strain, also used for deep mutational scanning) and a subtype B background (B1 strain) in an expression vector. The plasmids were generated by Twist Biosciences. Pseudoviruses were produced and neutralization was measured as previously described[55]. All F constructs included the full cytoplasmic tail and were paired with RSV G in an expression plasmid (AddGene: HDM_RSV_Long_G_31AACTdel Product ID 237350) for these transfections. All plasmid maps can be found here: https://github.com/dms-vep/RSV_Long_F_DMS/tree/main/supplemental_data/plasmids/.

Mutations impacting nirsevimab neutralization made in subtype A included (N67T, K68N, K68Q, D73N, K201S, K201T, P205S, V207E, K209D, K209Q, Q210T, S211R, S215K) and subtype B (K68N, K68Q, D73N, N201S, N201T, P205S, Q209D, Q210T, S211R, S215K). V207E did not produce usable pseudovirus titers in the B1 background. These are shown in Figure 3 and Supplemental Figure 4.

Mutations T67N and Q209K were also made in subtype B, which are mutations to the amino acid residue found in the subtype A Long strain. Data for these mutants along with the corresponding mutations in subtype A (N67T and K209Q) are shown in Supplemental Figure 4. Subtype A K68Q and K201S and subtype B K68Q and N201S are shown in Figures 1, 3 and Supplemental Figure 4.

The Long and B1 wildtype neutralization curves shown in Figure 3D,F are representative - all replicates can be found here https://github.com/dms-vep/RSV_Long_F_DMS/tree/main/non-pipeline_analyses/validations. The correlation plots in Figures 3 and 4 show fold change IC50 from wildtype using a matched wildtype from the specific experimental date for the mutations and the wildtype point plotted in the correlation plots is a geometric mean IC50 of all wildtype replicates.

Mutations impacting clesrovimab made in subtype A and B included R429M, R429S, S443P and G446D and are shown in Figure 4 and Supplemental Figure 5. Pseudoviruses expressing F called “A2020” and “B2024” in Supplemental Figure 5A are F sequences from natural strains that are broadly representative of recent subtype A and B strains[55], and have the GenBank accession numbers PP495954 and PP660445, respectively.

Interactive Nextstrain phylogenetic trees with antibody-escape scores

We integrated computer code into the Nextstrain[67] RSV view to enable scoring of natural RSV sequences for antibody resistance and visualization of the results on phylogenetic trees. A GitHub repository with the computer code implementing this scoring is at http://github.com/nextstrain/rsv. Briefly, the pre-existing Nextstrain view downloaded all RSV sequences from Pathoplexus[68] (currently >60,000), and built separate subtype A and B phylogenetic trees subsampled to roughly ~3,000 sequences designed to be representative across time and countries. We added computer code that assigns each of these sequences an “escape score” calculated from the deep mutational scanning data as either the sum of the effect of all of its constituent mutations or the max effect of any of its mutations on neutralization by the Fab or IgG form of nirsevimab or clesrovimab. The interactive phylogenetic trees can then be colored by these escape scores using the dropdown “Color By” option on the left toolbar (eg, see https://nextstrain.org/rsv/b/F-antibody-escape/6y?c=Nirsevimab-Fab_total_escape); there is also an option to label sequences by their top escape mutation. We integrated this scoring into the Nextstrain RSV builds for the F sequences and the full genome; note that there are also builds that emphasize different

bioRxiv preprint doi: https://doi.org/10.64898/2026.02.12.705519; this version posted February 12, 2026. The copyright holder for this preprint (which was not certified by peer review) is the author/funder, who has granted bioRxiv a license to display the preprint in perpetuity. It is made available under aCC-BY 4.0 International license.

timeframes: all-time, the last 6 years, and the last 3 years. The builds are updated to include the latest available sequences, so going to views linked above will show the latest sequence data.

We also created new builds called "F-antibody-escape" in the Nextstrain RSV views that shows trees subsampled to include all sequences with high nirsevimab or clesrovimab escape scores. Unlike the "F" builds, these "F-antibody-escape" builds over-represent the frequency of resistant strains. The "F-antibody-escape" trees do not provide an accurate view of the prevalence of resistance mutations; however, when you want to identify all of the top resistant strains (which otherwise could be dropped during subsampling) then these builds should be preferred. Which build is displayed can be selected using the "change dataset" option on the left toolbar.

Validation of strains with predicted neutralization resistance

A subset of natural RSV F sequences with predicted resistance to nirsevimab or clesrovimab neutralization identified using the 'Interactive Nextstrain phylogenetic trees with antibody-escape scores' were codon optimized and subsequently cloned into an expression vector by Twist Biosciences. F sequences with predicted resistance to nirsevimab Fab or IgG included (PP_002XVQT, PP_002KSRJ, PP_002QMLP, PP_002WHEU, PP_002WWH8, PP_002SUFP, PP_001QYN9, PP_001Y2UB, PP_003W55P). Sequences with predicted resistance to clesrovimab Fab or IgG included (PP_002W1BG, PP_001WGC0, PP_001Y62S, PP_001ZQ7W). PP_001W26S and PP_002UDSB correspond to subtype A and B controls also referred to in our prior study as A2020 and B2024, respectively[55]. A complete list of these key sequences are available in Pathoplexus under SeqSet PP_SS_628.1[91], and all sequences displayed in the trees in Figure 5 and Supplemental Figure 7 are available in Pathoplexus under SeqSet PP_SS_661.1[92] for subtype A and SeqSet PP_SS_662.1[93] for subtype B. All plasmid maps can be found at: https://github.com/dms-vep/RSV_Long_F_DMS/tree/main/supplemental_data/plasmids/strain%20validations. These were used to generate RSV pseudoviruses expressing the F from the natural sequences paired with RSV G expression plasmid (AddGene: HDM_RSV_Long_G_31AACTdel Product ID237350) as previously described[55]. Producing RSV pseudoviruses with F from natural sequences paired with all the same G ensures we do not introduce any variability from G. These pseudoviruses were then used in neutralization assays with nirsevimab or clesrovimab IgG and Fab[55]. To ensure reliable neutralization curves, we established a cut-off of 400,000 RLU/well for the no antibody, virus-only control. For strains with titers near the cut-off, extra controls were included to ensure escape was specific to the monoclonal antibody and not attributable to experimental artifacts.

Structural analysis

UCSF ChimaX[94] was used for structural visualizations. All Protein Data bank accession IDs used are included in figure legends.

Supplementary Appendix: biophysical model of how bivalent binding shapes impact of viral mutations on IgG versus Fab neutralization

Here we describe a biophysical model of how the effect of a mutation to a viral antigen on neutralization by an antibody depends on the antibody's affinity for the antigen. The two key effects modeled here are the bivalent binding of the IgG (but not Fab) and the ligand depletion (titration) that can put a floor on the

bioRxiv preprint doi: https://doi.org/10.64898/2026.02.12.705519; this version posted February 12, 2026. The copyright holder for this preprint (which was not certified by peer review) is the author/funder, who has granted bioRxiv a license to display the preprint in perpetuity. It is made available under aCC-BY 4.0 International license.

lowest measurable neutralization value. The model is illustrated conceptually in Figure 1A, and is used to generate the simulated data in Figure 1B that is compared to the actual experimental data in Figure 1C.

See https://github.com/jbloomlab/IgG-vs-Fab-neutralization for the computer code implementing the model, and https://jbloomlab.github.io/IgG-vs-Fab-neutralization/notebook.html for an interactive notebook describing the model.

Fab Binding

Let the binding affinity of the Fab have dissociation constant K_D. There are two states, unbound (U) and bound (B). The Boltzmann weights for these two states as a function of the molar concentration c of Fab are $w_U(c) = 1$ and $w_B(c) = \frac{c}{K_D}$. So the probability of the unbound state as a function of c is $p_U^{Fab}(c) = \frac{w_U(c)}{w_U(c) + w_B(c)} = \frac{1}{1 + c/K_D}$. This two-state partition-function formulation for monovalent binding follows classic multivalency treatments[95,96].

IgG binding

For the IgG, we assume each arm of the bivalent IgG has the same monovalent affinity for the viral antigen as the Fab described above. However, once the first arm binds, the effective concentration c_{eff} of the second arm is set by the density/spacing of viral antigens and the reach of the antibody. Here we do not consider those factors (antigen density, antibody reach, etc) separately, but just collapse them into the single effective concentration of the second arm after the first has bound, c_{eff}. The definition of an effective local concentration for the second arm, set by geometry/linker statistics rather than bulk concentration mirrors prior work[52,97,98]. In realistic scenarios, if bivalent binding is possible then $c_{eff} \gg c$ since the effective concentration of the second Fab arm in proximity to the viral antigen after the first arm has bound is much higher than the overall IgG concentration (note that concentrations should be in *molar* units rather than ng/ml in order to allow the same concentration scale to be used for Fab and IgG, since they have different molecular weights).

There are now three possible states, unbound (U), a single Fab arm bound (B_1), and both Fab arms bound (B_2). The Boltzmann weights for these three states as a function of the molecular concentration of IgG are $w_U(c) = 1$, $w_{B_1}(c) = \frac{c}{K_D}$, and $w_{B_2}(c) = \frac{c}{K_D} \times \frac{c_{eff}}{K_D}$. Further, note that state B_1 has a multiplicity of two since either of the Fab arms can bind[96]. So the probability of the unbound state as a function of c is (accounting for the multiplicity of two for B_1) is $p_U^{IgG}(c) = \frac{w_U(c)}{w_U(c) + 2w_{B_1}(c) + w_{B_2}(c)} = \frac{1}{1 + \frac{c}{K_D}\left(2 + \frac{c_{eff}}{K_D}\right)}$. Note that the effective dissociation constant of the IgG is $K_D^{IgG} = K_D / \left(2 + \frac{c_{eff}}{K_D}\right)$.

Assumption: binding affinity equals neutralization potency

In what follows, we assume that binding affinity equals neutralization potency, such that the neutralization IC50 of the Fab is equivalent to K_D. In other words, we equate fraction infectivity with fraction of viral epitopes (p_u); as described immediately below, deviations can occur under multi-hit models. Specifically, how fraction bound (binding affinity) relates to neutralization potency depends on how many antibodies must bind to a virion in order to neutralize it. The quantitative relationship

bioRxiv preprint doi: https://doi.org/10.64898/2026.02.12.705519; this version posted February 12, 2026. The copyright holder for this preprint (which was not certified by peer review) is the author/funder, who has granted bioRxiv a license to display the preprint in perpetuity. It is made available under aCC-BY 4.0 International license.

between binding affinity and neutralization potency as well as its impact on the neutralization curve slope can be modeled under assumptions about the number of spikes per virions and the number that must be bound to neutralize[99–103]. Here we are going to *ignore* this issue for now, and just conflate neutralization IC50 with Fab K_D. This is a quantitative simplification, but should not affect the main qualitative trends—and has the advantage of not requiring us to estimate difficult to determine quantities such as how many spikes there are per virion and what fraction of them must be bound for neutralization. Note that in the limiting case where this is just one spike per virion and binding one site on it is sufficient for neutralization, then ignoring this issue has no effect.

Estimating c_{eff} from the IgG versus Fab IC50

We can estimate c_{eff} (the parameter that describes the extent of avidity from bivalent binding) from the IC50 (or midpoint on the neutralization curve) of the IgG versus Fab. In particular, let m_{Fab} and m_{IgG} be the molar concentrations at the midpoint (IC50) of the Fab versus IgG neutralization curves, respectively. Then $K_D = m_{Fab}$ and $1/2 = \frac{1}{1+\frac{m_{IgG}}{m_{Fab}}\left(2+\frac{c_{eff}}{m_{Fab}}\right)}$. Solving for c_{eff} yields $c_{eff} = m_{Fab}\left(\frac{m_{Fab}}{m_{IgG}} - 2\right)$.

Impact of mutation(s)

Consider one or more mutations that cause a fold change in Fab IC50 of f_{mut}. For instance, a mutation that increases the Fab IC50 by 20-fold would have $f_{mut} = 20$. Note that mutations that cause a fixed change in the free energy of binding are expected to cause the same fold change in Fab IC50 in any genetic background. In the presence of these mutation(s), the fraction of Fab not neutralized becomes $p_U^{Fab}(c) = \frac{1}{1+\frac{c}{f_{mut}\times K_D}}$ and the fraction of IgG not neutralized becomes $p_U^{IgG}(c) = \frac{1}{1+\frac{c}{f_{mut}\times K_D}\left(2+\frac{c_{eff}}{f_{mut}\times K_D}\right)}$.

Complication: accounting for ligand depletion

Everything above is written in terms of the antibody (Fab or IgG) concentration c. In fact, c in these equations refers to the *free* concentration of antibody. But when the concentration of viral antigen is comparable to or exceeds the dissociation constant of the antibody (K_D for the Fab and K_D^{IgG} for the IgG), there can be "ligand depletion," which is the term we use here for when a large fraction of the antibody is bound to the viral antigen. When this occurs, much of the antibody gets "soaked up" by binding to viral antigen, and so the actual concentration of free antibody in the neutralization assay represented by c in the above equations is appreciably less than the total concentration added to the reaction. This phenomenon is nicely described in detail by Jarmoskaite et al (2020)[51], who refer to it as the "titration regime."

To quantitatively deal with this, we need to define some additional variables. Let c_{total} be the total antibody concentration added to the assay volume, let c_{free} be the concentration of antibody that is not bound to viral antigen (free), and let c_{bound} be the concentration of antibody that is bound to viral antigen. Also, let v_{total} be the total concentration of viral antigen (quantified in terms of number of the relevant epitope per unit volume), let v_{free} be the concentration of free viral antigen (not bound by antibody), and note that concentration of bound viral antigen is c_{bound}. We have the following equations: $c_{total} = c_{free} + c_{bound}$ (mass balance for the antibody), $v_{total} = v_{free} + c_{bound}$ (mass balance for the viral

bioRxiv preprint doi: https://doi.org/10.64898/2026.02.12.705519; this version posted February 12, 2026. The copyright holder for this preprint (which was not certified by peer review) is the author/funder, who has granted bioRxiv a license to display the preprint in perpetuity. It is made available under aCC-BY 4.0 International license.

antigen), and $c_{bound} \times K_D^{effective} = v_{free} \times c_{free}$ (there is an equilibrium with respect to the free antibody and antigen concentration). Note that for the Fab, $K_D^{effective} = K_D$ and for the IgG, $K_D^{effective} = K_D^{IgG}$.

Solving this system of three equations yields[51]

$c_{bound} = \left(c_{total} + v_{total} + K_D^{effective} - \sqrt{\left(c_{total} + v_{total} + K_D^{effective}\right) - 4c_{total} \times v_{total}}\right)/2$ and so

$c_{free} = c_{total} - c_{bound} = \left(c_{total} - v_{total} - K_D^{effective} + \sqrt{\left(c_{total} + v_{total} + K_D^{effective}\right) - 4c_{total} \times v_{total}}\right)/2.$

Note that in the limit where the viral antigen concentration is limiting and so we are outside the ligand depletion regime (eg, $v_{total} \ll K_D^{effective}$), then we just have $c_{free} \approx c_{total}$. However, when the viral antigen concentration is comparable to or greater than $K_D^{effective}$, then it is important to substitute c_{free} for c in all of the equations above.

We can also calculate the actual observed IC50s accounting for ligand depletion. The IC50 (under our assumption above that this is when half of viral epitopes are bound) occurs when $1/2 = c_{bound} / v_{total}$. It turns out that this can be neatly solved to determine the actual observed IC50 (accounting for ligand depletion) is $c_{IC50,observed} = K_D^{effective} + v_{total}/2$, whereas the ideal IC50 if there is no ligand depletion (when $v_{total} \ll K_D^{effective}$), is just $c_{IC50,ideal} = K_D^{effective}$. The floor on the measurable IC50 (eg, the lowest value that can be measured) is therefore $v_{total}/2$.

Realistic parameter estimates

We ballpark (these are rough estimates) realistic parameter values for nirsevimab and RSV F from our experiments (Figure 1C); the model-simulated data in Figure 1B use these parameters with the subtype A K_D estimates for the high-affinity panel and the subtype B K_D estimates for the low-affinity panel, and all other parameters shared between the panels as they are not expected to be subtype-specific. For the Fab IC50, which is represented by m_{Fab} or K_D in the above equations:

- subtype A (Long) strain: $K_D \sim 0.01$ nM
- subtype B (B1) strain: $K_D \sim 1$ nM

We also need to estimate c_{eff}; however, doing that is complicated by the fact that at least for subtype A, the IgG neutralization assays are likely in the ligand depletion range (what Jarmoskaite et al[51] call the "titration regime") where the IgG IC50 (m_{IgG}) cannot be measured accurately since the concentration of the viral antigen protein likely is comparable or greater to the true IgG IC50. So we will use neutralization measurements against the subtype B (B1) strain as any IgG ligand depletion should be less here due to the lower potency, and we assume that the actual avidity (potential for bivalent binding) captured in c_{eff} should not be strain dependent. Against this strain, we have m_{IgG} ~ 0.01 nM and m_{Fab} ~ 1 nM. So this gives c_{eff} ~ 100 nM. However, there is probably still ligand depletion in the measurement of m_{IgG} since the subtype B IgG neutralization is just as good as subtype A, so we will add another factor of 10 and use c_{eff} ~ 1000 nM (note this remains a very rough estimate and real value could be higher).

The hardest parameter to estimate is the number of viral epitopes v_{total} which determines if there is ligand depletion. Roughly, we might estimate 10^6 infectious particles per ml, with 10^2 non-infectious particles for each infectious one, 10^2 epitopes per particle. In that case, we have 10^{13} epitopes / liter,

bioRxiv preprint doi: https://doi.org/10.64898/2026.02.12.705519; this version posted February 12, 2026. The copyright holder for this preprint (which was not certified by peer review) is the author/funder, who has granted bioRxiv a license to display the preprint in perpetuity. It is made available under aCC-BY 4.0 International license.

which gives v_{total} ~ 0.01 nM. Note that this estimate, which was used in Figure 1B, is very much a rough estimate and could vary by an order of magnitude or more in either direction.

Interactive visualization of IgG and Fab neutralization and how it is affected by mutations

Go to https://jbloomlab.github.io/IgG-vs-Fab-neutralization/chart.html for an interactive chart initialized with the ballpark-realistic parameter values above for the subtype A strain of how nirsevimab neutralization differs between the Fab and IgG, and how this is impacted by mutations. In the interactive chart, you can use the sliders to adjust the Fab affinity (K_D), the avidity (c_{eff}), the effect of the viral mutation(s) (f_{mut}), and the viral epitope concentration (v_{total}). As you do so, you can see how the neutralization curves and IC50s change. Note for the IC50s, the interactive chart shows both the actual observed IC50 (accounting for ligand depletion) as well as what would be the ideal IC50 in the absence of any ligand depletion.

bioRxiv preprint doi: https://doi.org/10.64898/2026.02.12.705519; this version posted February 12, 2026. The copyright holder for this preprint (which was not certified by peer review) is the author/funder, who has granted bioRxiv a license to display the preprint in perpetuity. It is made available under aCC-BY 4.0 International license.

References

1. Li, Y. *et al.* Global, regional, and national disease burden estimates of acute lower respiratory infections due to respiratory syncytial virus in children younger than 5 years in 2019: a systematic analysis. *The Lancet* **399**, 2047–2064 (2022).
2. Mazur, N. I., Caballero, M. T. & Nunes, M. C. Severe respiratory syncytial virus infection in children: burden, management, and emerging therapies. *The Lancet* **404**, 1143–1156 (2024).
3. Suh, M. *et al.* Respiratory Syncytial Virus Is the Leading Cause of United States Infant Hospitalizations, 2009–2019: A Study of the National (Nationwide) Inpatient Sample. *J. Infect. Dis.* **226**, S154–S163 (2022).
4. RSV vaccines offer vital protection for the most vulnerable, study confirms. https://www.gavi.org/vaccineswork/rsv-vaccines-offer-vital-protection-most-vulnerable-study-confirms.
5. CDC. RSV Immunization Guidance for Infants and Young Children. *Respiratory Syncytial Virus Infection (RSV)* https://www.cdc.gov/rsv/hcp/vaccine-clinical-guidance/infants-young-children.html (2025).
6. Jones, J. M. *et al.* Use of Nirsevimab for the Prevention of Respiratory Syncytial Virus Disease Among Infants and Young Children: Recommendations of the Advisory Committee on Immunization Practices — United States, 2023. *MMWR Morb. Mortal. Wkly. Rep.* **72**, 920–925 (2023).
7. Moulia, D. L. *et al.* Use of Clesrovimab for Prevention of Severe Respiratory Syncytial Virus–Associated Lower Respiratory Tract Infections in Infants: Recommendations of the Advisory Committee on Immunization Practices — United States, 2025. *MMWR Morb. Mortal. Wkly. Rep.* **74**, 508–514 (2025).
8. Committee on Infectious Diseases *et al.* Recommendations for the Prevention of RSV Disease in Infants and Children: Policy Statement. *Pediatrics* **156**, e2025073923 (2025).
9. O'Leary, S. T. & Committee on Infectious Diseases. Recommended Childhood and Adolescent Immunization Schedule: United States, 2026: Policy Statement. *Pediatrics* https://doi.org/10.1542/peds.2025-075754 (2026) doi:10.1542/peds.2025-075754.
10. American Academy of Pediatrics. AAP Immunization Schedule. https://publications.aap.org/redbook/resources/15585/AAP-Immunization-Schedule (2026).
11. Xu, H. *et al.* Estimated Effectiveness of Nirsevimab Against Respiratory Syncytial Virus. *JAMA Netw. Open* **8**, e250380 (2025).
12. Payne, A. B. *et al.* Effectiveness of nirsevimab among infants in their first RSV season in the United States, October 2023–March 2024: a test-negative design analysis. *Lancet Reg. Health - Am.* **49**, 101196 (2025).
13. Pelletier, J. H. *et al.* Nirsevimab Administration and RSV Hospitalization in the 2024-2025 Season. *JAMA Netw. Open* **8**, e2533535 (2025).
14. Zambrano, L. D. *et al.* Nirsevimab Effectiveness Against Intensive Care Unit Admission for Respiratory Syncytial Virus in Infants — 24 States, December 2024–April 2025. *MMWR Morb. Mortal. Wkly. Rep.* **74**, 580–588 (2025).
15. Patton, M. E. *et al.* Interim Evaluation of Respiratory Syncytial Virus Hospitalization Rates Among Infants and Young Children After Introduction of Respiratory Syncytial Virus Prevention Products — United States, October 2024–February 2025. *MMWR Morb. Mortal. Wkly. Rep.* **74**, 273–281 (2025).
16. Bonavia, A. *et al.* RSM01, a novel respiratory syncytial virus monoclonal antibody: preclinical characterization and results of a first-in-human, randomised clinical trial. *BMC Infect. Dis.* **24**, 1378 (2024).
17. RSV vaccine and mAb snapshot. https://www.path.org/our-impact/resources/rsv-vaccine-and-mab-snapshot/.

bioRxiv preprint doi: https://doi.org/10.64898/2026.02.12.705519; this version posted February 12, 2026. The copyright holder for this preprint (which was not certified by peer review) is the author/funder, who has granted bioRxiv a license to display the preprint in perpetuity. It is made available under aCC-BY 4.0 International license.

18. Bizot, E. *et al.* Prophylactic monoclonal antibodies against respiratory syncytial virus in early life: An in-depth review of mechanisms of action, failure factors, and future perspectives. *Pediatr. Allergy Immunol.* **36**, e70257 (2025).
19. Al Gharaibeh, F., Deshmukh, V. & Deshmukh, H. Advances in RSV Immunoprophylaxis: Evolution, Efficacy, and Implementation Challenges. *NeoReviews* **26**, e704–e711 (2025).
20. McLellan, J. S. *et al.* Structure of RSV Fusion Glycoprotein Trimer Bound to a Prefusion-Specific Neutralizing Antibody. *Science* **340**, 1113–1117 (2013).
21. Zhu, Q. *et al.* A highly potent extended half-life antibody as a potential RSV vaccine surrogate for all infants. *Sci. Transl. Med.* **9**, eaaj1928 (2017).
22. Tang, A. *et al.* A potent broadly neutralizing human RSV antibody targets conserved site IV of the fusion glycoprotein. *Nat. Commun.* **10**, 4153 (2019).
23. Kistler, K. E. & Bedford, T. An atlas of continuous adaptive evolution in endemic human viruses. *Cell Host Microbe* **31**, 1898-1909.e3 (2023).
24. Zhu, Q. *et al.* Natural Polymorphisms and Resistance-Associated Mutations in the Fusion Protein of Respiratory Syncytial Virus (RSV): Effects on RSV Susceptibility to Palivizumab. *J. Infect. Dis.* **205**, 635–638 (2012).
25. Hause, A. M. *et al.* Sequence variability of the respiratory syncytial virus (RSV) fusion gene among contemporary and historical genotypes of RSV/A and RSV/B. *PLOS ONE* **12**, e0175792 (2017).
26. Simões, E. A. F. *et al.* Suptavumab for the Prevention of Medically Attended Respiratory Syncytial Virus Infection in Preterm Infants. *Clin. Infect. Dis.* **73**, e4400–e4408 (2021).
27. Nuttens, C. *et al.* Differences Between RSV A and RSV B Subgroups and Implications for Pharmaceutical Preventive Measures. *Infect. Dis. Ther.* **13**, 1725–1742 (2024).
28. Wilkins, D. *et al.* Nirsevimab binding-site conservation in respiratory syncytial virus fusion glycoprotein worldwide between 1956 and 2021: an analysis of observational study sequencing data. *Lancet Infect. Dis.* **23**, 856–866 (2023).
29. Ahani, B. *et al.* Molecular and phenotypic characteristics of RSV infections in infants during two nirsevimab randomized clinical trials. *Nat. Commun.* **14**, 4347 (2023).
30. Zhu, Q. *et al.* Prevalence and Significance of Substitutions in the Fusion Protein of Respiratory Syncytial Virus Resulting in Neutralization Escape From Antibody MEDI8897. *J. Infect. Dis.* **218**, 572–580 (2018).
31. Lin, G.-L. *et al.* Distinct patterns of within-host virus populations between two subgroups of human respiratory syncytial virus. *Nat. Commun.* **12**, 5125 (2021).
32. Fourati, S. *et al.* Genotypic and phenotypic characterisation of respiratory syncytial virus after nirsevimab breakthrough infections: a large, multicentre, observational, real-world study. *Lancet Infect. Dis.* S147330992400570X (2024) doi:10.1016/S1473-3099(24)00570-X.
33. U.S. Food and Drug Administration. *Beyfortus (Nirsevimab-Alip) Prescribing Informationl*. https://www.accessdata.fda.gov/drugsatfda_docs/label/2023/761328s000lbl.pdf (2025).
34. Fourati, S. *et al.* Real-World Emergence of Nirsevimab Resistance in RSV-B Breakthrough Infections. Preprint at https://doi.org/10.2139/ssrn.5427106 (2025).
35. Piñana, M. *et al.* Genomic evolution of human respiratory syncytial virus during a decade (2013–2023): bridging the path to monoclonal antibody surveillance. *J. Infect.* **88**, 106153 (2024).
36. LaVerriere, E. *et al.* Genomic Epidemiology of Respiratory Syncytial Virus in a New England Hospital System, 2024. *Open Forum Infect. Dis.* **12**, ofaf334 (2025).
37. Holland, L. A. *et al.* Genomic Sequencing Surveillance to Identify Respiratory Syncytial Virus Mutations, Arizona, USA. *Emerg. Infect. Dis.* **29**, (2023).
38. Evans, D. *et al.* Genomic Epidemiology of Human Respiratory Syncytial Virus, Minnesota, USA, July 2023–February 2024. *Emerg. Infect. Dis.* **30**, (2024).

bioRxiv preprint doi: https://doi.org/10.64898/2026.02.12.705519; this version posted February 12, 2026. The copyright holder for this preprint (which was not certified by peer review) is the author/funder, who has granted bioRxiv a license to display the preprint in perpetuity. It is made available under aCC-BY 4.0 International license.

39. Rice, A. *et al.* Human respiratory syncytial virus genetic diversity and lineage replacement in Ireland pre- and post-COVID-19 pandemic. *Microb. Genomics* **11**, (2025).
40. Köndgen, S. *et al.* A robust, scalable, and cost-efficient approach to whole genome sequencing of RSV directly from clinical samples. *J. Clin. Microbiol.* **62**, e01111-23 (2024).
41. Stobbelaar, K. *et al.* Functional implications of respiratory syncytial virus F sequence variability: a comparative analysis using contemporary RSV isolates. *mSphere* **10**, e00860-24 (2025).
42. Shishir, T. A. *et al.* Genome-wide study of globally distributed respiratory syncytial virus (RSV) strains implicates diversification utilizing phylodynamics and mutational analysis. *Sci. Rep.* **13**, 13531 (2023).
43. Lamichhane, B. *et al.* Respiratory Syncytial Virus Strain Evolution and Mutations in Western Australia in the Context of Nirsevimab Prophylaxis. *Open Forum Infect. Dis.* **12**, ofaf429 (2025).
44. Dong, X. *et al.* An Improved Rapid and Sensitive Long Amplicon Method for Nanopore-Based RSV Whole-Genome Sequencing. *Influenza Other Respir. Viruses* **19**, e70106 (2025).
45. Maloney, D. M. *et al.* ARTIC RSV amplicon sequencing reveals global RSV genotype dynamics. *Wellcome Open Res.* **10**, 323 (2025).
46. Nunley, B. E. *et al.* Clinical Performance Evaluation of a Tiling Amplicon Panel for Whole-Genome Sequencing of Respiratory Syncytial Virus. *J. Mol. Diagn.* **27**, 819–831 (2025).
47. Terstappen, J. *et al.* RSM01, an extended half-life RSV monoclonal antibody with a high barrier to resistance. Preprint at https://doi.org/10.64898/2026.02.04.703721 (2026).
48. Joyce, M. G. *et al.* Crystal Structure and Immunogenicity of the DS-Cav1-Stabilized Fusion Glycoprotein From Respiratory Syncytial Virus Subtype B. *Pathog. Immun.* **4**, 294 (2019).
49. McLellan, J. S., Ray, W. C. & Peeples, M. E. Structure and Function of Respiratory Syncytial Virus Surface Glycoproteins. in *Challenges and Opportunities for Respiratory Syncytial Virus Vaccines* (eds Anderson, L. J. & Graham, B. S.) vol. 372 83–104 (Springer Berlin Heidelberg, Berlin, Heidelberg, 2013).
50. Sun, Y. *et al.* A potent broad-spectrum neutralizing antibody targeting a conserved region of the prefusion RSV F protein. *Nat. Commun.* **15**, 10085 (2024).
51. Jarmoskaite, I., AlSadhan, I., Vaidyanathan, P. P. & Herschlag, D. How to measure and evaluate binding affinities. *eLife* **9**, e57264 (2020).
52. Einav, T., Yazdi, S., Coey, A., Bjorkman, P. J. & Phillips, R. Harnessing Avidity: Quantifying the Entropic and Energetic Effects of Linker Length and Rigidity for Multivalent Binding of Antibodies to HIV-1. *Cell Syst.* **9**, 466-474.e7 (2019).
53. Klein, J. S. & Bjorkman, P. J. Few and Far Between: How HIV May Be Evading Antibody Avidity. *PLoS Pathog.* **6**, e1000908 (2010).
54. Dadonaite, B. *et al.* A pseudovirus system enables deep mutational scanning of the full SARS-CoV-2 spike. *Cell* **186**, 1263-1278.e20 (2023).
55. Simonich, C. A. L. *et al.* RSV F evolution escapes some monoclonal antibodies but does not strongly erode neutralization by human polyclonal sera. *J. Virol.* **99**, e00531-25 (2025).
56. Casadevall, A., Roane, P. R., Shenk, T. & Roizman, B. The Story behind the Science: On the discovery of respiratory syncytial virus. *mBio* **16**, e03074-24 (2025).
57. Otwinowski, J., McCandlish, D. M. & Plotkin, J. B. Inferring the shape of global epistasis. *Proc. Natl. Acad. Sci.* **115**, (2018).
58. Haddox, H. K. *et al.* Jointly modeling deep mutational scans identifies shifted mutational effects among SARS-CoV-2 spike homologs. Preprint at https://doi.org/10.1101/2023.07.31.551037 (2023).
59. Rossey, I., McLellan, J. S., Saelens, X. & Schepens, B. Clinical Potential of Prefusion RSV F-specific Antibodies. *Trends Microbiol.* **26**, 209–219 (2018).
60. Gilman, M. S. A. *et al.* Rapid profiling of RSV antibody repertoires from the memory B cells of naturally infected adult donors. *Sci. Immunol.* **1**, eaaj1879 (2016).

bioRxiv preprint doi: https://doi.org/10.64898/2026.02.12.705519; this version posted February 12, 2026. The copyright holder for this preprint (which was not certified by peer review) is the author/funder, who has granted bioRxiv a license to display the preprint in perpetuity. It is made available under aCC-BY 4.0 International license.

61. Karron, R. A. *et al.* Respiratory syncytial virus (RSV) SH and G proteins are not essential for viral replication *in vitro* : Clinical evaluation and molecular characterization of a cold-passaged, attenuated RSV subgroup B mutant. *Proc. Natl. Acad. Sci.* **94**, 13961–13966 (1997).
62. U.S. Food and Drug Administration. *ENFLONSIA (Clesrovimab-Cfor) Prescribing Information*. https://www.accessdata.fda.gov/drugsatfda_docs/label/2025/761432s000lbl.pdf (2025).
63. Tabor, D. E. *et al.* Global Molecular Epidemiology of Respiratory Syncytial Virus from the 2017–2018 INFORM-RSV Study. *J. Clin. Microbiol.* **59**, e01828-20 (2020).
64. Bin Lu *et al.* Emergence of new antigenic epitopes in the glycoproteins of human respiratory syncytial virus collected from a US surveillance study, 2015–17. *Sci. Rep.* **9**, 3898 (2019).
65. Wetzke, M. *et al.* Prevalence of Resistance-Associated Mutations in RSV F Protein Against Monoclonal Antibodies Prior to Widespread Implementation: Findings From a Prospective German Pediatric Cohort. *Influenza Other Respir. Viruses* **19**, e70164 (2025).
66. Iglesias-Caballero, M. *et al.* Genomic Surveillance and Antigenic Characterization of Respiratory Syncytial Virus (RSV) in Spain During the 2023-2024 Season of Nirsevimab Administration. *J. Infect. Dis.* jiaf530 (2025) doi:10.1093/infdis/jiaf530.
67. Hadfield, J. *et al.* Nextstrain: real-time tracking of pathogen evolution. *Bioinformatics* **34**, 4121–4123 (2018).
68. Vecchia, E. D. Pathoplexus: towards fair and transparent sequence sharing. *Lancet Microbe* **5**, (2024).
69. Palivizumab, a humanized respiratory syncytial virus monoclonal antibody, reduces hospitalization from respiratory syncytial virus infection in high-risk infants. The IMpact-RSV Study Group. *Pediatrics* **102**, 531–537 (1998).
70. Zhu, Q. *et al.* Analysis of Respiratory Syncytial Virus Preclinical and Clinical Variants Resistant to Neutralization by Monoclonal Antibodies Palivizumab and/or Motavizumab. *J. Infect. Dis.* **203**, 674–682 (2011).
71. Zhao, X., Chen, F.-P. & Sullender, W. M. Respiratory syncytial virus escape mutant derived in vitro resists palivizumab prophylaxis in cotton rats. *Virology* **318**, 608–612 (2004).
72. Zhao, X. & Sullender, W. M. In Vivo Selection of Respiratory Syncytial Viruses Resistant to Palivizumab. *J. Virol.* **79**, 3962–3968 (2005).
73. Bates, J. T. *et al.* Escape from neutralization by the respiratory syncytial virus-specific neutralizing monoclonal antibody palivizumab is driven by changes in on-rate of binding to the fusion protein. *Virology* **454–455**, 139–144 (2014).
74. Adams, O. *et al.* Palivizumab-Resistant Human Respiratory Syncytial Virus Infection in Infancy. *Clin. Infect. Dis.* **51**, 185–188 (2010).
75. Antiviral Product Development — Conducting and Submitting Virology Studies to the Agency. (2006).
76. Li, Y. *et al.* 560. Efficacy and Safety of Retavibart, a Long-acting Monoclonal Antibody, for the Prevention of Respiratory Syncytial Virus-Induced Lower Respiratory Tract Infection: A Phase 2b Trial in Infants Entering Their First Epidemic Season. *Open Forum Infect. Dis.* **13**, ofaf695.169 (2026).
77. Sun, Y. *et al.* An antibody cocktail targeting conserved, nonoverlapping epitopes prevents viral escape and confers protection against RSV in vivo. *Sci. Transl. Med.* **18**, eady2450 (2026).
78. Bloom, J. D., Gong, L. I. & Baltimore, D. Permissive Secondary Mutations Enable the Evolution of Influenza Oseltamivir Resistance. *Science* **328**, 1272–1275 (2010).
79. Simonsen, L. *et al.* The Genesis and Spread of Reassortment Human Influenza A/H3N2 Viruses Conferring Adamantane Resistance. *Mol. Biol. Evol.* **24**, 1811–1820 (2007).
80. Chao, D. L., Bloom, J. D., Kochin, B. F., Antia, R. & Longini, I. M. The global spread of drug-resistant influenza. *J. R. Soc. Interface* **9**, 648–656 (2012).
81. Boundy, E. O. *et al.* Respiratory Syncytial Virus Immunization Coverage Among Infants Through Receipt of Nirsevimab Monoclonal Antibody or Maternal Vaccination — United States, October 2023–March 2024. *MMWR Morb. Mortal. Wkly. Rep.* **74**, 484–489 (2025).

bioRxiv preprint doi: https://doi.org/10.64898/2026.02.12.705519; this version posted February 12, 2026. The copyright holder for this preprint (which was not certified by peer review) is the author/funder, who has granted bioRxiv a license to display the preprint in perpetuity. It is made available under aCC-BY 4.0 International license.

82. Schickli, J. H., Kaur, J., Ulbrandt, N., Spaete, R. R. & Tang, R. S. An S101P Substitution in the Putative Cleavage Motif of the Human Metapneumovirus Fusion Protein Is a Major Determinant for Trypsin-Independent Growth in Vero Cells and Does Not Alter Tissue Tropism in Hamsters. *J. Virol.* **79**, 10678–10689 (2005).
83. Cantoni, D. *et al.* Correlation between pseudotyped virus and authentic virus neutralisation assays, a systematic review and meta-analysis of the literature. *Front. Immunol.* **14**, 1184362 (2023).
84. Humes, D., Rainwater, S. & Overbaugh, J. The TOP vector: a new high-titer lentiviral construct for delivery of sgRNAs and transgenes to primary T cells. *Mol. Ther. - Methods Clin. Dev.* **20**, 30–38 (2021).
85. Aditham, A. K. *et al.* Deep mutational scanning of rabies glycoprotein defines mutational constraint and antibody-escape mutations. *Cell Host Microbe* **33**, 988-1003.e10 (2025).
86. Dadonaite, B. *et al.* Deep mutational scanning of H5 hemagglutinin to inform influenza virus surveillance. Preprint at https://doi.org/10.1101/2024.05.23.595634 (2024).
87. Bloom, J. D. An Experimentally Determined Evolutionary Model Dramatically Improves Phylogenetic Fit. *Mol. Biol. Evol.* **31**, 1956–1978 (2014).
88. Yu, T. C. *et al.* Pleiotropic mutational effects on function and stability constrain the antigenic evolution of influenza haemagglutinin. *Nat. Ecol. Evol.* https://doi.org/10.1038/s41559-025-02895-1 (2025) doi:10.1038/s41559-025-02895-1.
89. Crawford, K. & Bloom, J. alignparse: A Python package for parsing complex features from high-throughput long-read sequencing. *J. Open Source Softw.* **4**, 1915 (2019).
90. Yu, T. C. *et al.* A biophysical model of viral escape from polyclonal antibodies. *Virus Evol.* **8**, veac110 (2022).
91. Pathoplexus. SeqSet: RSV_F_DMS_Validations. https://doi.org/10.62599/PP_SS_628.1 (2026).
92. Pathoplexus. SeqSet: RSV_A_F_sequences_for_tree. https://doi.org/10.62599/PP_SS_661.1 (2026).
93. Pathoplexus. SeqSet: RSV_B_F_sequences_for_tree. https://doi.org/10.62599/PP_SS_662.1 (2026).
94. Meng, E. C. *et al.* UCSF ChimeraX: Tools for structure building and analysis. *Protein Sci.* **32**, e4792 (2023).
95. Hlavacek, W. S., Posner, R. G. & Perelson, A. S. Steric Effects on Multivalent Ligand-Receptor Binding: Exclusion of Ligand Sites by Bound Cell Surface Receptors. *Biophys. J.* **76**, 3031–3043 (1999).
96. Perelson, A. S. & DeLisi, C. Receptor clustering on a cell surface. I. theory of receptor cross-linking by ligands bearing two chemically identical functional groups. *Math. Biosci.* **48**, 71–110 (1980).
97. Mammen, M., Choi, S.-K. & Whitesides, G. M. Polyvalent Interactions in Biological Systems: Implications for Design and Use of Multivalent Ligands and Inhibitors. *Angew. Chem. Int. Ed.* **37**, 2754–2794 (1998).
98. Fasting, C. *et al.* Multivalency as a Chemical Organization and Action Principle. *Angew. Chem. Int. Ed.* **51**, 10472–10498 (2012).
99. Magnus, C. Virus Neutralisation: New Insights from Kinetic Neutralisation Curves. *PLoS Comput. Biol.* **9**, e1002900 (2013).
100. Brandenberg, O. F. *et al.* Predicting HIV-1 transmission and antibody neutralization efficacy in vivo from stoichiometric parameters. *PLOS Pathog.* **13**, e1006313 (2017).
101. Pierson, T. C. *et al.* The Stoichiometry of Antibody-Mediated Neutralization and Enhancement of West Nile Virus Infection. *Cell Host Microbe* **1**, 135–145 (2007).
102. Klasse, P. J. Neutralization of Virus Infectivity by Antibodies: Old Problems in New Perspectives. *Adv. Biol.* **2014**, 1–24 (2014).
103. Yang, X., Kurteva, S., Lee, S. & Sodroski, J. Stoichiometry of Antibody Neutralization of Human Immunodeficiency Virus Type 1. *J. Virol.* **79**, 3500–3508 (2005).